A pan-variant mRNA-LNP T cell vaccine protects HLA transgenic mice from mortality after infection with SARS-CoV-2 Beta

Brandon Carter[1,10,+], Pinghan Huang[2,+], Ge Liu[1,10], Yuejin Liang[2], Paulo J.C. Lin[5], Bi-Hung Peng[3], Lindsay McKay[6], Alexander Dimitrakakis[1,10], Jason Hsu[3], Vivian Tat[4], Panatda Saenkham-Huntsinger[2], Jinjin Chen[7], Clarety Kaseke[8], Gaurav D. Gaiha[8,9], Qiaobing Xu[7], Anthony Griffiths[6], Ying K. Tam[5], Chien-Te K. Tseng[2,3,4,*], David K. Gifford[1,10,11,*]

1. MIT Computer Science and Artificial Intelligence Laboratory, Cambridge, MA, USA
2. Department of Microbiology and Immunology, The University of Texas Medical Branch, Galveston, TX, USA
3. Department of Neuroscience, Cell Biology, and Anatomy, The University of Texas Medical Branch, Galveston, TX, USA
4. Department of Pathology, The University of Texas Medical Branch, Galveston, TX, USA
5. Acuitas Therapeutics, Vancouver, BC, Canada
6. Boston University's National Emerging Infectious Diseases Laboratories, Boston, MA, USA
7. Department of Biomedical Engineering, Tufts University, Medford, MA, USA
8. Ragon Institute of MGH, MIT, and Harvard, Cambridge, MA, USA
9. Division of Gastroenterology, Massachusetts General Hospital, Boston, MA, USA
10. MIT Electrical Engineering and Computer Science, Cambridge, MA, USA
11. MIT Biological Engineering, Cambridge, MA, USA

* Correspondence to: sktseng@utmb.edu, gifford@mit.edu
+ These authors contributed equally to this work.

Abstract

Clinically licensed COVID-19 vaccines ameliorate viral infection by inducing vaccinee production of neutralizing antibodies that bind to the SARS-CoV-2 Spike protein to inhibit viral cellular entry (Walsh et al., 2020; Baden et al., 2021), however the clinical effectiveness of these vaccines is transitory as viral variants arise that escape antibody neutralization (Tregoning et al., 2021; Willett et al., 2022). Vaccines that solely rely upon a T cell response to combat viral infection could be transformational because they can be based on highly conserved short peptide epitopes that hold the potential for pan-variant immunity, but a mRNA-LNP T cell vaccine has not been shown to be sufficient for effective antiviral prophylaxis. Here we show that a mRNA-LNP vaccine based on highly conserved short peptide epitopes activates a $CD8^+$ and $CD4^+$ T cell response that prevents mortality in HLA-A*02:01 transgenic mice infected with the SARS-CoV-2 Beta variant of concern (B.1.351). In mice vaccinated with the T cell vaccine, 24% of the nucleated cells in lung were $CD8^+$ T cells on day 7 post infection. This was 5.5 times more $CD8^+$ T cell infiltration of the lungs in response to infection compared to the Pfizer-BioNTech

Comirnaty® vaccine. Between days 2 and 7 post infection, the number of $CD8^+$ T cells in the lung increased in mice vaccinated with the T cell vaccine and decreased in mice vaccinated with Comirnaty®. The T cell vaccine did not produce neutralizing antibodies, and thus our results demonstrate that SARS-CoV-2 viral infection can be controlled by a T cell response alone. Our results suggest that further study is merited for pan-variant T cell vaccines, and that T cell vaccines may be relevant for individuals that cannot produce neutralizing antibodies or to help mitigate Long COVID.

Main

Current strategies for COVID-19 vaccine design utilize one or more SARS-CoV-2 Spike protein subunits to primarily activate the humoral arm of the adaptive immune response to produce neutralizing antibodies to the Spike receptor binding domain (RBD) (Walsh et al., 2020; Baden et al., 2021). Vaccination to produce neutralizing antibodies is a natural objective, as neutralizing antibodies present an effective barrier to the viral infection of permissive cells by binding to the RBD and thus blocking cellular entry via the ACE2 receptor. However, the strategy of focusing on Spike as the sole vaccine target has proven problematic as Spike rapidly evolves to produce structural variants that evade antibody-based acquired immunity from vaccination or infection with previous viral variants (Tregoning et al., 2021; Willett et al., 2022). Compared to the original Wuhan variant, novel viral variants are arising that are more contagious (Zhang et al., 2021), and infectious to a broader range of host species (Shuai et al., 2021). Thus, vaccine designers are pursuing a stream of novel Spike variant vaccines. Multivalent Spike vaccines and bivalent booster vaccines provide protection against multiple known variants of concern (VOC) of SARS-CoV-2 but are not necessarily protective against unknown future variants (Martinez et al., 2021). Mosaic RBD nanoparticles that display disparate SARS-CoV RBDs have been found to produce effective neutralizing antibodies against both SARS-CoV-1 and SARS-CoV-2 (Cohen et al., 2022), but the robustness of mosaic RBD protection against possible future Spike mutations depends upon conserved Spike structural epitopes. In contrast, the vaccine approach we present here depends upon conserved T cell epitopes drawn from the entire viral proteome for protection against future variants.

We show in this study that an immunogenic T cell vaccine with 11 conserved short MHC displayed epitopes (“MIT-T-COVID vaccine”) provides effective prophylaxis against the onset of SARS-CoV-2-induced morbidity and mortality caused by SARS-CoV-2 Beta infection in

transgenic mice carrying human HLA-A*02:01. We demonstrate the MIT-T-COVID vaccine causes significant infiltration of $CD8^+$ and $CD4^+$ T lymphocytes in the lungs. Multiple designs for T cell vaccines for SARS-CoV-2 have been proposed (Liu et al., 2020; Nathan et al., 2021; Heitmann et al., 2022; Pardieck et al., 2022) and are in clinical trials (NCT05113862, NCT0488536, NCT05069623, NCT04954469), but identifying the mechanisms behind the efficacy of pure T cell vaccines remains an open question. Substantial literature suggests that T cell responses are integral to the adaptive immunity to COVID-19 (Moss, 2022). For example, a study that ablated the B cell compartment of the immune system in Spike vaccinated mice found that $CD8^+$ T cells alone can control viral infection (Israelso et al., 2021). Pardieck et al. (2022) found that vaccination with a single $CD8^+$ T cell epitope conferred protection against mortality from the Leiden-0008/2020 SARS-CoV-2 variant in K18-hACE2 transgenic mice, but unlike our study, required three doses for efficacy, did not engage a $CD4^+$ T cell response, and did not identify significant T cell infiltration of the lungs. In addition to specific antibody responses, COVID-19 vaccinees and convalescent patients possess SARS-CoV-2 specific $CD8^+$ and $CD4^+$ T cells, suggesting the contribution of the T cell compartment to the adaptive immunity to COVID-19 (Sekine et al., 2020), and clinical findings have revealed vaccine-induced T cell responses in B cell-deficient patients (Shree, 2022). It has also been reported that vaccination by WA (Wuhan) Spike in a mouse model failed to produce antibodies fully capable of neutralizing the SA (Beta) variant of CoV-2, yet immunized mice were protected against Beta strain challenge, leading to the conclusion that T cell responses were sufficient to control Beta SARS-CoV-2 (Kingstad-Bakke et al., 2022). In addition, vaccination with T cell epitope-rich Nucleocapsid protein produced specific T cell responses thought to be causally associated with viral control (Matchett et al., 2021). Intranasal vaccination of mice with SARS-CoV-1 Nucleocapsid followed by challenge with 10^4 Plaque-forming units of SARS-CoV-1 prevented mortality in 75% of the mice (Zhao et al, 2016). Combined Spike and Nucleocapsid vaccination improved viral control compared to Spike vaccination alone in preclinical models, while $CD8^+$ T cell depletion demonstrated the role of $CD8^+$ T cells in viral control and protection from weight loss (Hajnik et al., 2022).

Vaccine Design

We designed a COVID-19 T cell vaccine using T cell epitopes that are unchanged over 19 presently known SARS-CoV-2 variants of concern (VOC) (Methods). Since T cell epitopes can

113 originate from any part of the viral proteome, they can be drawn from portions of the proteome
114 that are likely to be evolutionarily stable. The prediction of stable epitopes can be
115 accomplished by historical analysis of thousands of viral variants (Liu et al., 2020), structural
116 analysis (Nathan et al., 2021), or the functional analysis of mutations lethal to the virus.
117 Beginning with stable epitopes as candidates, our T cell vaccine design proceeds by vaccine
118 epitope selection that optimizes population coverage where every vaccinated individual is
119 predicted to experience on average multiple immunogenic peptide-HLA hits (Liu et al., 2021; Liu
120 et al., 2022).
121
122 The MIT-T-COVID vaccine realizes an *n-times* coverage objective by encoding multiple
123 epitopes for each target MHC class I and II diplotype to (1) expand diverse sets of T cell
124 clonotypes to fight viral infection, (2) accommodate variations in epitope immunogenicity
125 between vaccinees, and (3) reduce the chances that viral evolution will lead to immune system
126 escape (Liu et al., 2022). The MIT-T-COVID vaccines consists of eight MHC class I epitopes
127 and three MHC class II epitopes (Figure 1A, Methods, Supplemental Table 1). The MHC class
128 I and II vaccine peptides are encoded into a single mRNA construct for delivery with the same
129 Acuitas LNP delivery platform that is used by the Pfizer-BioNTech Comirnaty® vaccine (Figure
130 1A). The eight MIT-T-COVID MHC class I epitopes are the HLA-A*02:01 subset of the MHC
131 class I *de novo* MIRA only vaccine design of Liu et al. (2021) that used combinatorial
132 optimization to select vaccine epitopes to maximize *n-times* population coverage over HLA
133 haplotype frequencies (Liu et al., 2022). For inclusion in the assembled construct, the eight
134 MHC class I vaccine peptides were randomly shuffled, and alternate peptides were flanked with
135 five additional amino acids at each terminus as originally flanked in the SARS-CoV-2 proteome.
136 Selected epitopes were flanked to test if flanking enhanced or impaired epitope presentation.
137 The three MHC class II epitopes were selected by considering all SARS-CoV-2 proteome
138 windows of length 13-25 and selecting conserved peptides that are predicted to be displayed by
139 the mouse MHC class II allele H-2-IAb (Methods). The mRNA construct encodes a secretion
140 signal sequence at the N-terminus and an MHC class I trafficking signal (MITD) at the C-
141 terminus (Kreiter et al., 2008). Peptide sequences are joined by non-immunogenic
142 glycine/serine linkers (Sahin et al., 2017). The construct also included control peptides for HLA-
143 A*02:01 and H-2-IAb (CMV pp65: NLVPMVATV for HLA-A*02:01 and Human CD74:
144 KPVSKMRMATPLLMQAL for H-2-IAb) (Vita et al., 2018).
145
146 **Challenge Study**

147

148 We vaccinated with three test articles: a negative control injection (PBS), the Pfizer-BioNTech
149 Comirnaty® vaccine (wastage that was refrozen and then thawed), and the MIT-T-COVID
150 vaccine (Figure 1B). We vaccinated HLA-A*02:01 human transgenic mice with these three
151 vaccines, vaccinating 11 age-matched male mice with each vaccine. Comirnaty® or MIT-T-
152 COVID vaccinations contained of 10 μg of mRNA. The mice were vaccinated at Day 0 and
153 boosted at Day 21 (Methods). At Day 35 three mice from each group were sacrificed for
154 immunogenicity studies, and at Day 37 the remaining eight mice were challenged intranasally
155 (I.N.) with 5 x 10^4 $TCID_{50}$ of the SARS-CoV-2 B.1.351 variant. Challenged mice were subjected
156 to daily monitoring for the onset of morbidity (i.e., weight changes and other signs of illness) and
157 any mortality. At Day 39 (2 days post infection) three mice were taken from each group and
158 sacrificed to determine viral burdens and to perform lung histopathology. At Day 44 (7 days
159 post infection) the remaining mice were sacrificed to determine viral burdens and to perform
160 lung histopathology.
161
162 **Immunogenicity of vaccines**
163
164 Vaccination by the MIT-T-COVID vaccine expanded $CD8^+$ and $CD4^+$ T cells that expressed
165 interferon gamma (IFN-γ) or tumor necrosis factor alpha (TNF-α) when queried by vaccine
166 epitopes (Figures 2A-B). The observed variability of immunogenicity of MIT-T-COVID epitopes
167 in convalescent COVID patients (Supplemental Table 1) and in the present study supports our
168 use of multiple epitopes per MHC diplotype for *n-times* coverage. Vaccination by Comirnaty®
169 produced no significant T cell responses to vaccine epitopes when compared to PBS. $CD8^+$ T
170 cells that are activated by the CD8-4 epitope (YLQPRTFLL, Spike 269-277) are expanded in
171 animals vaccinated with the MIT-T-COVID vaccine (IFN-γ 1.316% ± 0.529% of $CD8^+$ T cells, P
172 = 0.0087 vs. PBS; TNF-α 0.380% ± 0.086% of $CD8^+$ T cells, P = 0.0149 vs. PBS; Figure 2A).
173 Similarly, the CD8-8 epitope (TVYSHLLLV, ORF3a 89-97) activated $CD8^+$ T cells that are
174 expanded by the MIT-T-COVID vaccine (IFN-γ 0.560% ± 0.021% of $CD8^+$ T cells, P = 0.001 vs.
175 PBS; TNF-α 0.250% ± 0.125% of $CD8^+$ T cells, P = 0.015 vs. PBS) and the CD4-2 epitope
176 (RFYFYTSKTTVASLIN, ORF1ab 1421-1436) activated $CD4^+$ T cells are expanded by the MIT-
177 T-COVID vaccine (TNF-α 0.078% ± 0.027%, P = 0.058 vs. PBS, P = 0.010 vs. Comirnaty®,
178 IFN-γ not significant, Figure 2B). The lack of HLA-A*02:01 transgenic animal response to
179 certain $CD8^+$ epitopes that were immunogenic in patients (Supplemental Table 1) is consistent

180 with past studies of transgenic mouse models (Kotturi et al., 2009) and the variability of
181 immunogenicity of epitopes between in-bred mice (Croft et al., 2019).
182
183 T cells that lack IFN-γ responses can produce effective immune mediators (Nakiboneka et al.,
184 2019). We found that the fraction of $CD4^+$ T cells that are $FoxP3^+$ were not expanded in
185 Comirnaty® or MIT-T-COVID vaccinated animals, suggesting that fraction of T regulatory cells
186 that could induce tolerance were not expanded by vaccination (Figure 2C).
187
188 **Vaccine efficacy against the onset of morbidity and mortality and the viral loads in**
189 **challenged mice**
190
191 Upon viral challenge, both PBS and MIT-T-COVID vaccinated animals exhibited a more than
192 10% weight loss by Day 3 (PBS mean weight reduction 11.386% ± 1.688%, MIT mean weight
193 reduction 10.851% ± 0.641%), with the MIT-T-COVID vaccinated animals beginning to recover
194 from Day 4 onward (Figure 3A). The weight phenotype was mirrored by the clinical score
195 phenotype, with PBS animals not recovering and MIT-T-COVID vaccinated animals improving
196 from Day 5 onward (Figure 3B, Methods). The Comirnaty® vaccine protected animals from
197 significant weight loss and poor clinical scores.
198
199 When the yields of infectious progeny virus were measured at 2 days post infection (dpi), we
200 noted that mice immunized with MIT-T-COVID vaccine had 6.706 ± 0.076 log10 $TCID_{50}$/g,
201 compared to 7.258 ± 0.367 log10 $TCID_{50}$/g in the PBS control, representing a moderate 3.6-fold
202 reduction in viral replication (P = 0.046; Figure 3D). In contrast, mice immunized with
203 Comirnaty® had infectious viral titers that were below the detection limits at 2 dpi. Infectious
204 viral titer was not significant for all test articles at 7 dpi (Figure 3D). Lung viral mRNA levels
205 measured by qPCR followed the same trends as infectious virus progeny in the lungs, with
206 Comirnaty® showing no significant levels. Despite a reduced content of total and sub-genomic
207 viral RNAs associated with MIT-T-COVID vaccine samples as assessed by qPCR, the reduction
208 was insignificant, compared to those of PBS control (Supplemental Figure 1).
209
210 All the Comirnaty® and MIT-T-COVID vaccine animals survived to 7 dpi, when the study was
211 terminated, with the difference in clinical scores of these two vaccine groups becoming
212 insignificant (Figure 3C). In contrast, four of five PBS control animals had been euthanized

213 because of weight loss > 20%. The survival of all five animals vaccinated with Comirnaty®
214 and the MIT-T-COVID vaccine was significant vs. PBS (P = 0.0053, logrank test).
215
216 We noted that mice immunization with the Comirnaty® vaccine elicited substantial specific
217 antibodies capable of completely neutralizing Beta and WA-1 variants of CoV-2 with 100%
218 neutralizing titers (NT_{100}) of 896 ± 350 and fold 2048 ± 1887, respectively (Figure 3E). The
219 higher neutralizing titer against WA-1 is expected as it is variant matched to Comirnaty®. As
220 expected for a peptide-based vaccine, no neutralizing titer could be readily detected in the
221 serum from mice immunized with MIT-T-COVID vaccine or PBS. Total specific IgG/IgM
222 antibodies were also measured by ELISA against a cell lysate prepared from WA-1-infected
223 Vero E6 cells. Comirnaty® has a log10 IgG/IgM titer of 4.915 ± 0.213, while the log10 titer
224 produced by PBS was 2.452 ± 0.321 and the MIT-T-COVID vaccine produced a log10 titer of
225 2.266 ± 0.291 (Figure 3F). The low but detectable titers in PBS and MIT-T-COVID vaccine-
226 immunized mice may represent an early IgM response to viral infection.
227
228 All lung samples were subjected to immunohistochemistry (IHC) staining for SARS-CoV-2 spike
229 protein (Supplemental Figure 2). We found specimens vaccinated with PBS exhibited extensive
230 staining indicative of viral infection throughout the epithelium of both the bronchioles and the
231 alveolar sacs, with the viral infection appearing more intense at 2 dpi. Although viral infection is
232 significantly reduced by 7 dpi, viral antigen was still readily detectable throughout alveoli. In
233 comparison, specimens vaccinated with the MIT-T-COVID vaccine exhibited similarly extensive
234 viral infection at 2 dpi throughout the bronchiolar and alveolar epithelia, albeit somewhat
235 reduced in intensity. However, by 7 dpi, viral infection was significantly reduced in both extent
236 and intensity, with brown puncta being detected only in a few alveoli scattered throughout the
237 tissue. Contrasted with both PBS and MIT-T-COVID vaccinated specimens, the Comirnaty®-
238 vaccinated specimens exhibited significantly reduced viral infections at both 2 and 7 dpi. Apart
239 from a single area at 7 dpi (see Supplemental Figure 3), viral antigen was undetected at both
240 timepoints in Comirnaty® vaccinated animals.
241
242 Paraffin-embedded and H&E-stained lung specimens of differentially immunized mice,
243 harvested at 2 and 7 dpi, were subjected to histopathological examination (Supplemental Figure
244 4). We found that at 7 dpi mice immunized with MIT-T-COVID vaccine exhibited extensive
245 lymphocytic infiltrations in perivascular regions and spaces from around bronchi, bronchioles, to
246 alveoli. Fewer infiltrations were found in mice immunized with either Comirnaty® or PBS.

247 Additionally, these infiltrations only localized at perivascular regions around bronchi and large
248 bronchioles. Despite the less intensive and localized inflammatory infiltrates, we also noted
249 widespread congestion, hemorrhage, and few foci of thromboembolism were exclusively
250 observed within the lungs of Comirnaty®-immunized mice but not others (Supplemental Figure
251 4). We also noted the lung histopathology was milder but the same pattern at 2 dpi than those of
252 7 dpi (data not shown).
253
254 Lung specimens were subjected to IHC staining for $CD8^+$ and $CD4^+$ cells at both 2 and 7 dpi
255 (Figure 4; Supplemental Figures 5-7). At 2 dpi, we found a significant increase in $CD8^+$ T cells
256 infiltrating the lungs in mice immunized with MIT-T-COVID (12.6% ± 5.91% of all nucleated cells
257 were $CD8^+$) or Comirnaty® (12.4% ± 2.35%) compared to mice immunized with PBS (PBS
258 mean 4.48% ± 1.99%; $P = 0.044$ vs. MIT-T-COVID, $P = 0.050$ vs. Comirnaty®; Figure 4A).
259 At 7 dpi, we found a significant increase in $CD8^+$ T cells infiltrating the lungs in mice immunized
260 with MIT-T-COVID (24.0% ± 5.21% of all nucleated cells were $CD8^+$) compared to mice
261 immunized with Comirnaty® (Comirnaty® mean 4.35% ± 2.20%, $P = 0.001$) or PBS (PBS mean
262 7.32% ± 4.88%, $P = 0.001$; Figure 4A). We observed a significant increase in $CD8^+$ T cells
263 infiltrating the lungs in mice immunized with MIT-T-COVID between 2 and 7 dpi ($P = 0.0039$),
264 and a significant decrease in $CD8^+$ T cells infiltrating the lungs in mice immunized with
265 Comirnaty® between 2 and 7 dpi ($P = 0.044$; Figure 4A). At 7 dpi, we also found a significant
266 increase in $CD4^+$ T cells in filtrating the lungs in mice immunized with MIT-T-COVID (7.09% ±
267 4.05%) compared to mice immunized with PBS (PBS mean 0.41% ± 0.39%; $P = 0.0062$; Figure
268 4B).
269
270 **Discussion**
271
272 Existing Spike vaccines produce a T cell response that is thought to be important for vaccine
273 effectiveness and durability (Moss, 2022). However, the T cell response induced by a Spike
274 vaccine may be less effective in promoting durable immune responses than the T cell response
275 induced by a pure T cell vaccine. Spike based T cell responses may contain epitopes that are
276 subject to evolutionary change (de Silva et al., 2021; Redd et al., 2021), or Spike epitopes may
277 not be as well presented or immunogenic as epitopes drawn from a more diverse set of SARS-
278 CoV-2 proteins. Thus, T cell augmentation strategies for Spike vaccines (Liu et al., 2021) and
279 pure T cell vaccines will require further exploration to unravel the hierarchy of immune
280 responses to their components, and how to structure a vaccine for optimal prophylaxis. In

281 patients with impaired antibody responses, T cell vaccines would eliminate the burden of non-
282 immunogenic B cell epitopes (Benjamini et al., 2022) and provide immune protection, at least to
283 a certain extent, against infection.
284
285 The marginal IgG/IgM antibody titers that were not neutralizing elicited by mice immunized with
286 the MIT-T-COVID vaccine indicates that the protective mechanism of the vaccine was likely
287 based on a T cell response to the virus. The reduction in viral titer on day 2 shows that T cell
288 responses were present early in infection. In the absence of neutralizing antibodies these
289 responses were sufficient to rescue the vaccinated mice from the onset of mortality.
290
291 We expect that a T cell vaccine would provide prophylaxis similar to what we have described
292 against future SARS-CoV variants and strains that conserve the vaccine's epitopes. We chose
293 Beta (B.1.351) for our challenge study as it has a severe phenotype in a wild-type mouse
294 background (Shuai et al., 2021). Transgenic human ACE2 (hACE2) mice exhibit encephalitis
295 post COVID infection that does not represent human pathology (Kumari et al., 2021) and thus
296 may be a poor model for T cell vaccine effectiveness. Instead, we chose to evaluate the HLA-
297 A*02:01 component of our vaccine design in a HLA-A*02:01 transgenic animal model given the
298 predominance of HLA-A02 in the human population (Ellis et al., 2000).
299
300 The MIT-T-COVID vaccine induced a response where circulating T cells migrated rapidly and
301 efficiently into the lung upon viral challenge, as evidenced by more intense and widespread
302 lymphocytic infiltrations than other groups. Further, the degree of $CD8^+$ T cell infiltration of the
303 lungs significantly increased in mice vaccinated with the MIT-T-COVID vaccine between days 2
304 and 7 post infection, and significantly decreased in mice vaccinated with the Comirnaty®
305 vaccine. The lack of this T cell response in Comirnaty® vaccinated animals merits further study.
306
307 Another finding is that widespread congestion, hemorrhage, and few foci of thromboembolism
308 were exclusively observed within the lungs of Comirnaty®-immunized mice. Although this
309 finding is unrelated to the MIT-T-COVID vaccine, it suggests the possibility of immunization-
310 induced side-effects or immunopathology of mRNA-based CoV-2 vaccines. The exact
311 mechanism of pulmonary embolism in this case remains unknown for now and should be
312 explored.
313

Cytotoxic T cells ($CD8^+$ T cells) have the ability to kill virally infected cells, and thus T cell vaccines might provide long-term immunity and be effective therapeutics for Long COVID. Post-acute sequelae of COVID-19 (PASC, “Long COVID”) causes persistent symptoms in ~10% of people past twelve weeks of COVID infection (WHO, 2021). Long COVID has been associated with the continued presence of Spike in the blood, suggesting that a tissue based viral reservoir remains in Long COVID patients (Swank et al., 2022).

Our results suggest that if one goal of a vaccine is protection against novel viral strains it may be appropriate to develop vaccines that permit symptomatic infection but protect against severe illness. Current regulatory criteria for licensing vaccines are solely based upon the prevention of symptomatic illness for vaccine matched viral strains. Further research on T cell vaccines may reveal novel vaccine designs that prevent severe illness while providing protection against viral variants as an additional tool in the fight against global pandemics.

327 **A**

328

MRVTAPRTLILLLSGALALTETWAGS G G S G G G G S G G **YLYALVYFL** G G S G G G G S G G **RSKNPLLYDANYFLCWHTN**
G G S G G G G S G G **FVDGVPFVV** G G S G G G G S G G **AYYVGYLQPRTFLLKYNEN** G G S G G G G S G G
FLNRFTTTL G G S G G G G S G G **RLTKYTMADLVYALRHFDE** G G S G G G G S G G **SIIAYTMSL** G G S G G G G S G G
LLLFVTVYSHLLLVAAGLE G G S G G G G S G G **ATSRTLSYY** G G S G G G G S G G **KTFPPTEPK** G G S G G G G S G G
EEIAIILASFSASTSAFVETVKGLDY G G S G G G G S G G **KSILSPLYAFASEAARVVRSIFSRTL** G G S G G G G S G G
VDYGARFYFYTSKTTVASLINTLNDLGGSGGGGSGG**NLVPMVATV**GGSGGGGSGG**KPVSKMRMATPLLMQAL**GGSLGGGG
SGIVGIVAGLAVLAVVVIGAVVATVMCRRKSSGGKGGSYSQAASSDSAQGSDVSLTA

329

330

331 **B**

332

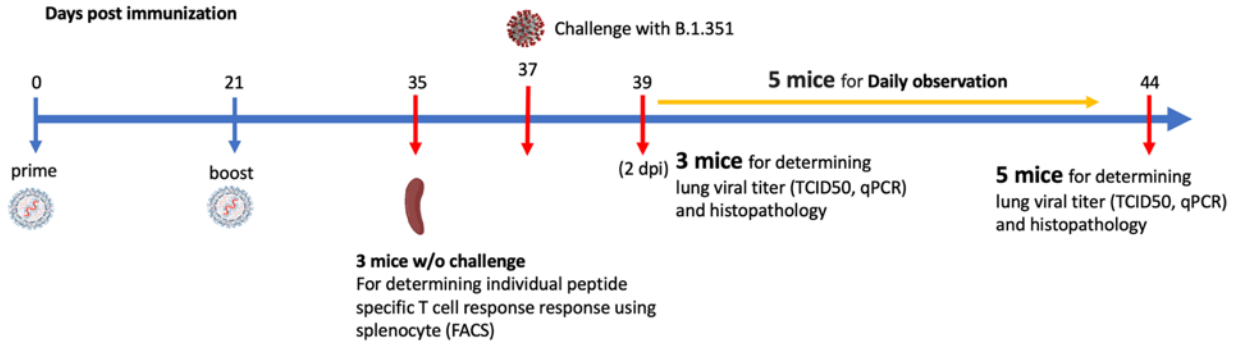

333

334

335 **Figure 1.** (A) Assembled vaccine construct containing a secretion signal sequence (red),
336 peptides (bold) joined by non-immunogenic glycine/serine linkers, and an MHC class I trafficking
337 signal (blue). (B) Study design.

338

339

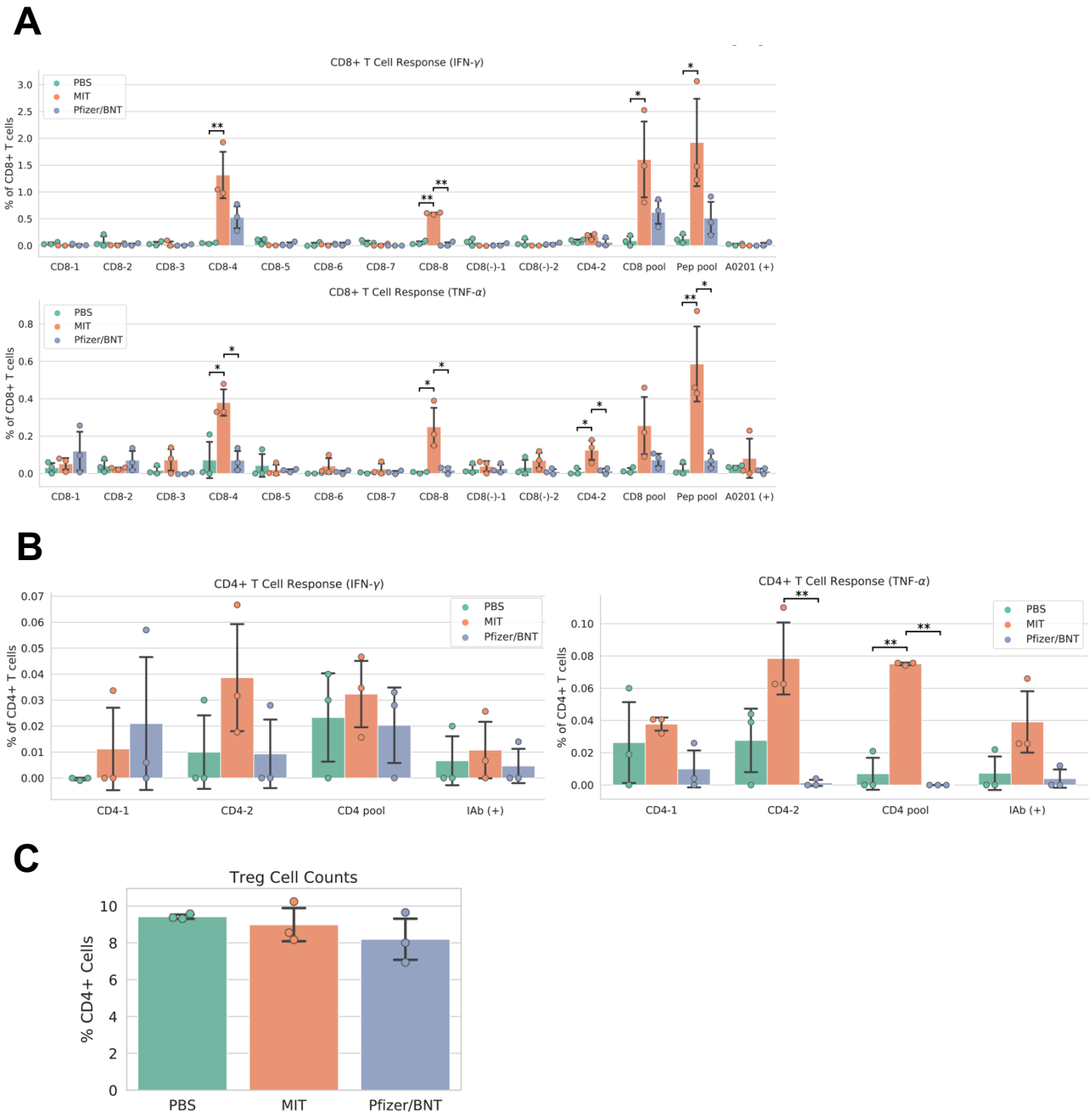

Figure 2. Vaccine immunogenicity. (A) CD8$^+$ T cell responses, (B) CD4$^+$ T cell responses, (C) FoxP3$^+$ T Regulatory cells as a percentage of all CD4$^+$ cells. The CD8 pool includes MHC class I peptides CD8-1—CD8-8 (Supplemental Table 1). The CD4 pool includes MHC class II peptides CD4-1 and CD4-2. The Pep pool includes all query peptides in Supplemental Table 1. Error bars indicate the standard deviation around each mean. *P* values were computed by one-way ANOVA with Tukey's test. **P* < 0.05, ***P* < 0.01.

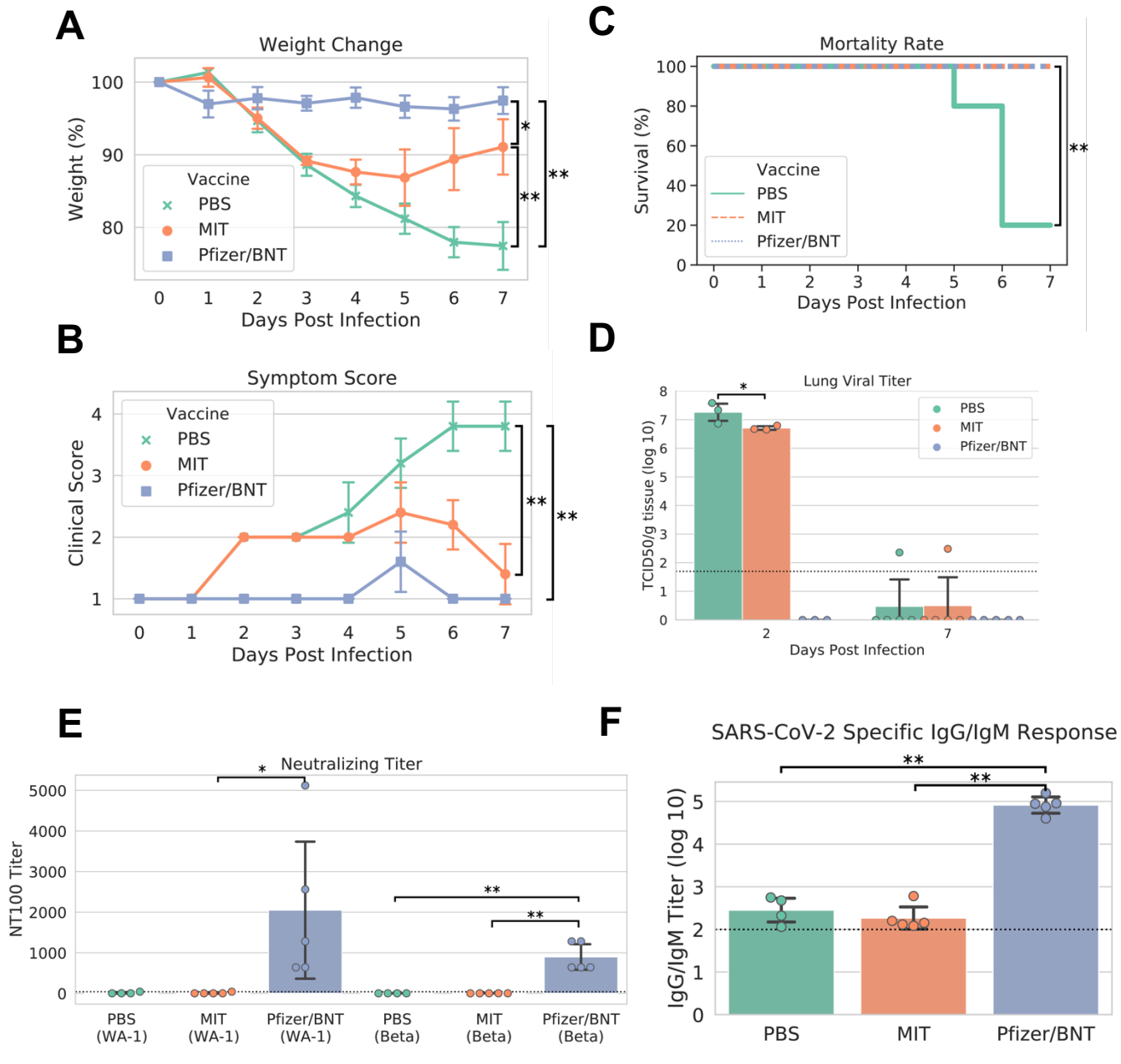

Figure 3. Study phenotypic data, lung viral titer, and vaccine antibody responses. (A) Weights vs. days post infection, (B) clinical scores vs. days post infection, (C) Kaplan-Meier mortality curve (mortality at 80% weight loss), (D) lung viral titer, (E) maximum serum dilution that provided 100% neutralization of viral infection *in vitro*, (F) IgG/IgM titer measured by ELISA against cell lysate infected with WA-1 SARS-CoV-2. Dotted lines in (D)-(F) indicate assay limits of detection. Error bars indicate the standard deviation around each mean. *P* values were computed by one-way ANOVA with Tukey's test except (C) *P* values were computed using the logrank test. $^{*}P < 0.05$ and $^{**}P < 0.01$.

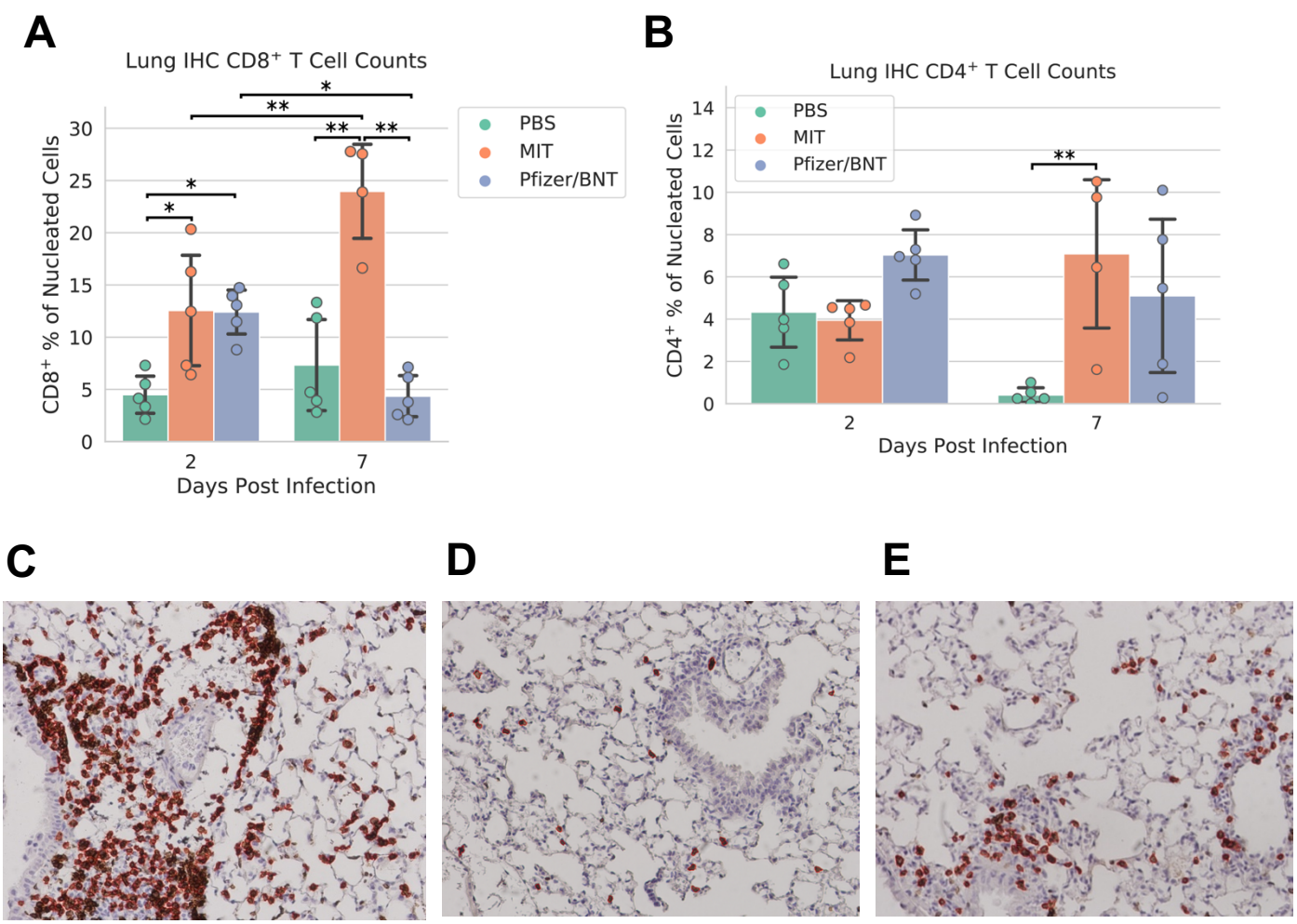

Figure 4. Lung immunohistochemistry for CD8$^+$ and CD4$^+$ cells. Counts of (A) CD8$^+$ and (B) CD4$^+$ T cells in expressed as a percentage of all nucleated cells visible in each field from lung tissue. Example CD8$^+$ stain images at 7 dpi for (C) MIT-T-COVID, (D) Pfizer/BNT, and (E) PBS vaccinated animals. Lung samples were subjected to IHC staining for CD8 (brown) with hematoxylin counterstain (blue). Images were taken at 10x magnification. Red outlines in (C)-(E) indicate CD8$^+$ cells identified and counted by CellProfiler software (Methods). Error bars indicate the standard deviation around each mean. *P* values were computed by two-way ANOVA with Tukey's test. *$P < 0.05$ and **$P < 0.01$. See also Supplemental Figures 5-7.

430 **Methods**

431

432 Mice

433

434 A total of 33 male HLA-A*02:01 human transgenic mice (Taconic 9659) were used that were
435 between 12 and 16 weeks old when they received their initial vaccination. These CB6F1
436 background mice carry the MHC class I alleles HLA-A*02:01, H-2-Kb, H-2-Db, H-2-Kd, and H-2-
437 Dd, and H-2-Ld. The mice carry the MHC class II alleles H-2-IAd, H-2-IEd, and H-2-IAb.

438

439 Tissue culture and virus

440

441 Vero E6 cells (ATCC, CRL:1586) were grown in minimum essential medium (EMEM, Gibco)
442 supplemented with penicillin (100 units/mL), streptomycin (100 µg/mL) and 10% fetal bovine
443 serum (FBS). Two strains of SARS-CoV-2 were used in this study, SARS-CoV-2 (US_WA-
444 1/2020 isolate) and Beta (B.1.351/SA, Strain: hCoV-19/USA/MD-HP01542/2021). Both viruses
445 were propagated and quantified in Vero E6 cells and stored at -80 °C until needed.

446

447 MIT-T-COVID vaccine design

448

449 MHC Class I epitopes. Eight peptides from SARS-CoV-2 were selected as a subset of the MHC
450 class I *de novo* MIRA only vaccine design of Liu et al., 2021. We filtered this set of 36 peptides
451 to the 8 peptides predicted to be displayed by HLA-A*02:01 by a combined MIRA and machine
452 learning model of peptide-HLA immunogenicity (Liu et al., 2021). The combined model predicts
453 which HLA molecule displayed a peptide that was observed to be immunogenic in a MIRA
454 experiment, and uses machine learning predictions of peptide display for HLA alleles not
455 observed or peptides not tested in MIRA data. Thus, all eight MHC class I peptides in our
456 vaccine were previously observed to be immunogenic in data from convalescent COVID-19
457 patients (Snyder et al., 2021). We further validated that all peptides are predicted to bind HLA-
458 A*02:01 with high (less than or equal to 50 nM) affinity using the NetMHCpan-4.1 (Reynisson et
459 al., 2020) and MHCflurry 2.0 (O'Donnell et al., 2020) machine learning models. For inclusion in
460 the assembled construct, the eight vaccine peptides were randomly shuffled, and alternate
461 peptides were flanked with five additional amino acids at each terminus as originally flanked in
462 the SARS-CoV-2 proteome. The CD4-2 vaccine epitope produced a $CD8^+$ response, and this
463 may be a consequence of a contained MHC class I epitope, with candidates including

464 SLINTLNDL (HLA-A*02:01 predicted binding 55 nM), ASLINTLNDL (H-2-Db predicted binding
465 289 nM), FYTSKTTVASL (H-2-Kd predicted binding 293 nM), FYFYTSKTTV (H-2-Kd predicted
466 binding 40 nM), and YFYTSKTTV (H-2-Kd predicted binding 56 nM).
467
468 MHC Class II epitopes. Three peptides from SARS-CoV-2 were optimized for predicted binding
469 to H-2-IAb. We scored all SARS-CoV-2 peptides of length 13-25 using the sliding window
470 approach of Liu et al. (2020) and a machine learning ensemble that outputs the mean predicted
471 binding affinity (IC50) of NetMHCIIpan-4.0 (Reynisson et al., 2020) and PUFFIN (Zeng et al.,
472 2019). We selected the top three peptides by predicted binding affinity using a greedy selection
473 strategy with a minimum edit distance constraint of 5 between peptides to avoid selecting
474 overlapping windows. All three peptides were flanked with an additional five amino acids per
475 terminus from the SARS-CoV-2 proteome.
476
477 The start and end amino acid positions of each vaccine peptide in its origin gene is shown in
478 Supplemental Table 1. For SARS-CoV-2, peptides are aligned to reference proteins in UniProt
479 (UniProt Consortium, 2019) (UniProt IDs: P0DTC2 (S), P0DTC3 (ORF3a), P0DTC5 (M),
480 P0DTC9 (N), P0DTD1 (ORF1ab)). All of the epitopes are conserved over these variants of
481 concern: Alpha (B.1.1.7), Beta (B.1.351), Gamma (P.1), Delta (21A, 21J, B.1.617.2), Kappa
482 (B.1.617.1), Epsilon (B.1.427, B.1.429), Iota (B.1.526), Lambda (C.37), Mu (B.1.621) , Omicron
483 (BA.1, BA.2, BA.4, B.5, BA.2.12.1, BA.2.75), EU1 (B.1.177).
484
485 MIT-T-COVID vaccine formulation
486
487 Codon optimization for mouse expression of the MIT-T-COVID vaccine construct was performed
488 using the IDT Codon Optimization Tool (Integrated DNA Technologies). The resulting nucleic
489 acid sequence is provided in Supplemental Table 2. RNA was synthesized by TriLink
490 BioTechnologies as a modified mRNA transcript with full substitution of 5-Methoxy-U, capped
491 (Cap 1) using CleanCap® AG and polyadenylated (120A). RNA containing lipid nanoparticles
492 were prepared as previously described (Pardi et al., 2017). Briefly, an ethanolic solution of
493 ALC-0315 (Patent WO2017075531), cholesterol, distearoylphosphatidylcholine (DSPC), and 2-
494 [(polyethylene glycol)-2000] N,N ditetradecylacetamide (ALC-0159, Patent Application
495 US14732218) was rapidly mixed with an solution of RNA in citrate buffer at pH 4.0 (composition
496 described in Patent WO2018081480). Physical properties of the LNP such as size and

497 polydispersity were assessed by Malvern Zetasizer and encapsulation efficiency by Ribogreen
498 assay (Life Technologies).
499
500 Animal vaccination and virus challenge
501
502 Thirty-three HLA-A*02:01 human transgenic mice were randomly divided into three groups and
503 immunized twice at three-week intervals with vehicle (PBS/300 mM sucrose), 10 µg of
504 Comirnaty® vaccine or 10 µg of MIT-T-COVID vaccine. All vaccines were administered as a
505 50 µl intramuscular injection. The Comirnaty® vaccine was wastage vaccine that was diluted for
506 human administration (0.9% NaCl diluent), and remaining unusable wastage vaccine in vials
507 was flash frozen at -80 °C. This wastage vaccine was later thawed and immediately
508 administered without dilution (50 ul is 10 ug of mRNA). No Comirnaty® was used that could
509 have been administered to humans. Since Comirnaty® was thawed twice, our results may not
510 be representative of its best performance. The MIT-T-COVID vaccine was diluted to 10 µg in
511 50 µL with PBS with 300 mM sucrose and then administered. At two weeks post booster
512 immunization, eight mice of each group were challenged with 5 x 10^4 $TCID_{50}$/60 µL of SARS-
513 CoV-2 (B.1.351/SA, Strain: hCoV-19/USA/MD-HP01542/2021) via intranasal (IN) route. Mice
514 were weighted daily and clinically observed at least once daily and scored based on a 1–4
515 grading system that describes the clinical wellbeing. Three mice in each group were euthanized
516 at 2 dpi for assessing viral loads and histopathology of the lung. The remaining five mice were
517 continued monitored for weight changes, other signs of clinical illness, and mortality (if any) for
518 up to 7 dpi before euthanasia for assessing antibody responses within the blood and viral loads
519 and histopathology of the lung. Animal studies were conducted at Galveston National
520 Laboratory at University of Texas Medical Branch at Galveston, Texas, based on a protocol
521 approved by the Institutional Animal Care and Use Committee at UTMB at Galveston.
522
523 Assessment of mortality and morbidity
524
525 Differentially immunized and challenged mice were monitored at least once each day for the
526 morbidity and mortality and assigned the clinical scores based on the following: 1: Healthy, 2:
527 ruffled fur, lethargic. 3: hunched posture, orbital tightening, increased respiratory rate, and/or >
528 15% weight loss, and 4: dyspnea and/or cyanosis, reluctance to move when stimulated or >
529 20% weight loss.
530

531 Immunogenicity measurements

532

533 At 14 days post booster immunization, three mice of each group were sacrificed for harvesting
534 splenocytes in 2ml R10 medium (RPMI, 10% FBS, 1%P/S, 10 mM HEPES). Briefly, spleens
535 were homogenized and subjected to filtration onto 40 μm cell strainers, followed by a wash of
536 strainers with 10 mL PBS and centrifuged at 500 g for 5 min at 4 °C. Cell pellet was
537 resuspended by using 2 mL of red blood cell lysis buffer (Thermo Fisher Scientific) for 2-3 min,
538 followed by a supplement of 20 mL PBS. Resulting cell suspensions were centrifuged at 500 g
539 for 5 min, resuspended in 2 mL R10 medium before counting the numbers under a microscope.
540 For a brief in vitro stimulation, aliquots of 10^6 cells were incubated with indicated peptide at a
541 final concentration of 1 μg/mL in each well of a 96-well plate. Golgiplug (5 μg/mL, BD
542 Bioscience) was added into the culture at 1 hr post stimulation and followed by an additional 4
543 hrs incubation. For cell surface staining, cultured splenocytes were resuspended in 40 μL FACS
544 buffer containing fluorochrome-conjugated antibodies and incubated 1 hr at 4 °C followed by cell
545 fixation using Cytofix/Cytoperm buffer (BD Bioscience) for 20 min at 4 °C. Cells were further
546 incubated with fluorochrome-conjugated cytokine antibodies overnight. The next day, cells were
547 washed twice using 1 × Perm/Wash buffer and resuspended in 300 μL FACS buffer for analysis.
548 For Foxp3 staining, cells were fixed and permeabilized by Foxp3/Transcription Factor Staining
549 Buffer Set (Thermo Fisher Scientific) according to the instruction. Fixable Viability Dye
550 eFluor506 (Thermo Fisher Scientific) was also used in all sample staining to exclude dead cells
551 from our data analysis. The fluorochrome-conjugated anti-mouse antibodies were listed as
552 below: FITC-conjugated CD3 (17A2, Biolegend), efluor450-conjugated CD4 (GK1.5,
553 eBioscience), PE-Cy7-conjugated CD8 (53-6.7, eBioscience), PE-conjugated IFN-γ (XMG1.2,
554 eBioscience), PerCP-eFlour710- conjugated TNF-α (MP6-XV22, eBioscience). For the Foxp3
555 staining, Pacific Blue-conjugated CD4 (GK1.5), FITC-conjugated CD25 (PC61), Percp-Cy5.5-
556 conjugated CTLA4 (UC-10-4B9), PE-conjugated Foxp3 (FJK-16s). Cell acquisition was
557 performed a BD LSR Fortessa and data were analyzed via FlowJo software version 10 (BD
558 Bioscience).

559

560 Viral titer assay

561

562 For virus quantitation, the frozen lung specimens were weighed before homogenization in
563 PBS/2% FBS solution using the TissueLyser (Qiagen), as previously described (Tseng et al.,
564 2007). The homogenates were centrifuged to remove cellular debris. Cell debris-free

565 homogenates were used to quantifying infectious viruses in the standard Vero E6 cell-based
566 infectivity assays in 96-well microtiter plates, as we routinely used in the lab (Tseng et al.,
567 2012). Titers of virus were expressed as 50% tissue culture infectious dose per gram of tissue
568 ($TCID_{50}$/g).
569
570 Antibody neutralization assay
571
572 Sera of mice collected at 7 dpi were used for measuring specific antibody responses. Briefly,
573 sera were heat-inactivated (56 °C) for 30 min, were stored at -80 °C until needed. For
574 determining the SARS-CoV-2 neutralizing antibody titers, serially two-fold (starting from 1:40)
575 and duplicate dilutions of heat-inactivated sera were incubated with 100 TCID of SARS-CoV-2
576 (US_WA-1/2020 isolate) or Beta (B.1.351/SA, Strain: hCoV-19/USA/MD-HP01542/2021) at 37
577 °C for 1 h before transferring into designated wells of confluent Vero E6 cells grown in 96-well
578 microtiter plates. Vero E6 cells cultured with medium with or without virus were included as
579 positive and negative controls, respectively. After incubation at 37 °C for 3 days, individual wells
580 were observed under the microscopy for the status of virus-induced formation of cytopathic
581 effect. The 100% neutralizing titers (NT_{100}) of sera were expressed as the lowest dilution folds
582 capable of completely preventing the formation of viral infection-induced cytopathic effect in
583 100% of the wells.
584
585 Serum IgG/IgM response by ELISA
586
587 ELISA was applied to verified serum IgG and IgM responses with SARS-CoV-2 (US_WA-1/2020
588 isolate) infected Vero-E6 cell lysate. In brief, SARS-CoV-2 infected Vero-E6 cell lysate was
589 coated on 96-well plate (Corning) at 1 μg/well in PBS for overnight at 4 °C. The plates were
590 blocked using 1% BSA/PBST for 1 h at room temperature. The 5-fold serial-dilution serum from
591 each mouse (starting at 1:100) was then added into antigen-coated plates and incubated for 1 h
592 at 37 °C. The plates were then washed three times with PBST (PBS/0.1% Tween-20) followed
593 by incubation with 100 μL of anti-mouse IgG and IgM HRP conjugated secondary antibody
594 (Jackson immunoresearch) (1:2000) for 1 h at 37 °C. After three times wash using PBST, 100
595 μL of ABTS substrate (Seracare) was added to the plates and incubated for 30 min in the dark.
596 After stopped by adding 1% SDS. Then absorbance at 405 nm (OD 405 nm) was measured
597 with the plate reader (Molecular Devices) and analyzed with GraphPad Prism Version 9.1.2.
598

599 RNA extraction and quantitative RT-PCR
600
601 Lung tissues were weighted and homogenized in 1 mL of Trizol reagent (Invitrogen) using
602 TissueLyser (Qiagen). The RNA was then extracted using Direct-zol RNA miniprep kits (Zymo
603 research) according to the manufacturer's instructions. 500 ng total RNA was then applied to
604 cDNA synthesis using iScript cDNA Synthesis kit (Biorad) according to the manufacturer's
605 instructions. The viral genomic RNA, subgenomic RNA and mice 18s rRNA has then been
606 amplified using iQ SYBR green supermix (Biorad) and performed using CFX96 real time system
607 (Biorad). The samples were run in duplicate using the following conditions: 95 °C for 3 min then
608 45 cycles of 95 °C for 15 s and 58 °C for 30 s. The level of expression was then normalized with
609 18s rRNA and calculated using $2^{-\Delta Ct}$ method, as we have previously described (Tseng et al.,
610 2007; Agrawal et al., 2015)
611
612 The primer set for SARS-CoV-2 RNA amplification is nCoV-F
613 (ACAGGTACGTTAATAGTTAATAGCGT) and nCoV-R (ATATTGCAGCAGTACGCACACA).
614 SgLeadSARS2-F (CGATCTCTTGTAGATCTGTTCTC) and nCoV-R
615 (ATATTGCAGCAGTACGCACACA) were used for subgenomic SARS-CoV-2 RNA
616 amplification. Mouse 18s rRNA was served as the internal control and amplified using 18s-
617 F(GGACCAGAGCGAAAGCATTTGCC) and 18s-R (TCAATCTCGGGTGGCTGAACGC).
618
619 Immunohistochemistry
620
621 All slides were prepared by the Histopathology Core (UTMB) into 5 μm paraffin-embedded
622 sections for immunohistochemistry (IHC). IHC staining and analysis were performed by UTMB
623 according to previously published protocols (Tseng et al., 2007; Yoshikawa et al., 2009). In
624 brief, a standard IHC sequential incubation staining protocol was followed to detect the SARS-
625 CoV-2 spike (S) protein, $CD4^+$ cells, or $CD8^+$ cells using a rabbit-raised anti-SARS-CoV-2 S
626 protein antibody (1:5000 dilution, ab272504, Abcam plc, Cambridge UK), a rabbit monoclonal
627 anti-CD4 antibody (1:250 dilution, ab183685, ab183685, Abcam plc, Cambridge, UK), and a
628 rabbit monoclonal anti-CD8 antibody (1:500 dilution, ab217344, Abcam plc, Cambridge, UK)
629 followed by peroxidase-conjugated secondary antibody and 3,3'-Diaminobenzidine (DAB)
630 substrate kit (MP-7802, Vector Laboratories, Burlingame, CA). Slides were counterstained with
631 hematoxylin (MHS16-500ML, Sigma-Aldrich Inc., St. Louis, MO) and antigen expression was
632 examined under 10X and 40X magnifications using an Olympus IX71 microscope.

$CD4^+$ and $CD8^+$ cell counts were quantified using CellProfiler 4.2.4 (Stirling et al., 2021). The image analysis pipeline included the following modules: (1) UnmixColors (for each of DAB and hematoxylin stains), (2) ImageMath (applied to DAB stain images only; subtract 0.5 from all intensity values and set values less than 0 equal to 0), and (3) IdentifyPrimaryObjects (require object diameter 20-60 pixels [DAB stain] or 15-60 pixels [hematoxylin stain]; Global threshold strategy; Otsu thresholding method with two-class thresholding, threshold smoothing scale 1.3488, threshold correction factor 1.0, lower threshold bound 0.0, upper threshold bound 1.0, no log transform before thresholding; Shape method to distinguish clumped objects and draw dividing lines between clumped objects; automatically calculate size of smoothing filter for declumping; automatically calculate minimum allowed distance between local maxima; speed up by using lower-resolution image to find local maxima; fill holes in identified objects after declumping only; continue handling objects if excessive number of objects identified).

Statistical Analysis

One-way ANOVA tests were performed in Python using the SciPy package (Virtanen et al., 2020). Two-way ANOVA and Tukey's tests were performed in Python using the statsmodels package (Seabold and Perktold, 2010). Logrank tests were performed using GraphPad Prism.

Acknowledgements

This work was supported in part by Schmidt Futures and a C3.ai grant to DG. We benefited from thoughtful comments from Michael Birnbaum.

Declaration of Interests

DG and BC are founders of Think Therapeutics. PL and YT are employees of Acuitas Therapeutics.

664 **Supplemental Data**

665

MHC Class	Vaccine Peptide	Query Peptide	Query ID	Organism	Gene	Vaccine Peptide Start-End	Query Peptide Start-End	MIRA	MCMT
1	YLYALVYFL	YLYALVYFL	CD8-1	SARS-CoV-2	ORF3a	107-115	107-115	0.86	0.19
1	RSKNPLLYDANYFL CWHTN	LLYDANYFL	CD8-2	SARS-CoV-2	ORF3a	134-152	139-147	0.70	0.44
1	FVDGVPFVV	FVDGVPFVV	CD8-3	SARS-CoV-2	ORF1ab	4726-4734	4726-4734	0.68	
1	AYYVGYLQPRTFLL KYNEN	YLQPRTFLL	CD8-4	SARS-CoV-2	S	264-282	269-277	0.66	0.62
1	FLNRFTTTL	FLNRFTTTL	CD8-5	SARS-CoV-2	ORF1ab	3482-3490	3482-3490	0.53	
1	RLTKYTMADLVYAL RHFDE	TMADLVYAL	CD8-6	SARS-CoV-2	ORF1ab	4510-4528	4515-4523	0.44	
1	SIIAYTMSL	SIIAYTMSL	CD8-7	SARS-CoV-2	S	691-699	691-699	0.59	
1	LLLFVTVYSHLLLV AAGLE	TVYSHLLLV	CD8-8	SARS-CoV-2	ORF3a	84-102	89-97	0.61	
1	ATSRTLSYY	ATSRTLSYY	CD8(-)-1	SARS-CoV-2	M	171-179	171-179		
1	KTFPPTEPK	KTFPPTEPK	CD8(-)-2	SARS-CoV-2	N	361-369	361-369		
1	NLVPMVATV	NLVPMVATV	A0201 (+)	CMV	pp65	495-503	495-503		
2	KSILSPLYAFASEA ARVVRSIFSRTL	PLYAFASEAARVVR SI	CD4-1	SARS-CoV-2	ORF1ab	527-552	532-547		
2	VDYGARFYFYTSKT TVASLINTLNDL	RFYFYTSKTTVASL IN	CD4-2	SARS-Cov-2	ORF1ab	1416-1441	1421-1436		
2	EEIAIILASFSAST SAFVETVKGLDY	–	Synthesis failed	SARS-CoV-2	ORF1ab	471-496	-		
2	KPVSKMRMATPLLM QAL	KPVSKMRMATPLLM QAL	IAb (+)	Homo sapiens	CD74	102-118	102-118		

666

667 **Supplemental Table 1.** MIT-T-COVID vaccine peptides, query peptides (vaccine
668 immunogenicity), peptide origin, and appearance probability in HLA-A*02:01 convalescent
669 COVID-19 patients in Snyder et al. (2020) (MIRA column) and Kared et al. (2021) (MCMT).
670 Selected peptides were tested by other studies for their immunogenicity in convalescent
671 COVID-19 patients whose HLA type included HLA-A*02:01. The study by Snyder et al. (2020)
672 included 80 HLA-A*02:01 convalescent COVID-19 patients and tested peptides individually or in
673 small pools with the Multiplex Identification of T-cell Receptor Antigen Specificity (MIRA) assay.
674 Query peptides were first filtered to only consider those with predicted HLA-A*02:01 binding
675 affinity less than or equal to 25 nM. The MIRA fraction in Supplemental Table 1 is the number
676 of individuals positive for a pool containing a query peptide divided by 80. The Kared et al.
677 (2021) study evaluated 16 HLA-A*02:01 convalescent COVID-19 patient by mass cytometry–

based multiplexed tetramer (MCMT) staining. The MCMT fraction in Supplemental Table 1 is the number of individuals positive for a query peptide divided by 16.

ATG AGG GTC ACA GCT CCT CGG ACC TTG ATC CTC CTT TTG TCT GGT GCT CTT
GCA CTG ACT GAG ACT TGG GCC GGG TCA GGA GGC AGT GGA GGA GGA GGA TCC
GGG GGT TAT TTG TAT GCT CTG GTT TAT TTT CTG GGC GGG TCC GGA GGC GGT
GGC TCT GGC GGG AGG TCC AAG AAT CCA CTT CTC TAC GAC GCA AAC TAT TTC
TTG TGT TGG CAC ACC AAT GGG GGG AGC GGT GGC GGA GGA AGC GGT GGG TTC
GTG GAC GGA GTT CCC TTT GTT GTT GGT GGG TCA GGC GGA GGA GGC TCT GGC
GGG GCT TAC TAT GTA GGG TAC CTG CAG CCC CGA ACA TTC CTT TTG AAA TAC
AAC GAG AAC GGT GGA TCC GGT GGG GGA GGA AGT GGA GGG TTT CTG AAT AGA
TTC ACC ACC ACT CTG GGA GGT TCT GGC GGC GGG GGT TCT GGT GGA CGG CTG
ACT AAA TAC ACA ATG GCC GAT CTT GTT TAC GCA TTG CGG CAT TTT GAT GAG
GGA GGC AGT GGC GGA GGG GGA TCC GGC GGC AGC ATA ATA GCT TAC ACC ATG
TCA CTG GGA GGG AGC GGA GGG GGC GGG AGC GGC GGT TTG CTC CTT TTC GTG
ACA GTG TAT AGC CAT CTC CTT CTG GTG GCA GCT GGC CTT GAA GGG GGG AGC
GGT GGA GGA GGT AGC GGT GGC GCC ACT TCT AGG ACA TTG AGT TAC TAT GGG
GGC AGC GGA GGA GGA GGT TCT GGA GGC AAG ACC TTC CCC CCT ACA GAG CCC
AAG GGA GGT TCC GGC GGC GGG GGC AGT GGT GGG GAA GAG ATC GCC ATT ATC
TTG GCT TCC TTT AGT GCT TCA ACA AGC GCT TTT GTA GAG ACC GTA AAG GGC
CTC GAT TAT GGA GGT TCA GGG GGA GGA GGC TCA GGT GGG AAG TCA ATA CTG
TCT CCT CTT TAT GCA TTT GCA TCA GAG GCT GCA AGA GTT GTC CGA TCC ATT TTT
TCT CGC ACT CTT GGG GGG TCC GGC GGA GGC GGG TCT GGC GGT GTG GAT TAT
GGT GCT AGG TTT TAT TTT TAC ACT TCC AAA ACC ACT GTT GCC TCT CTC ATA AAT
ACC CTC AAT GAC CTG GGA GGG TCT GGT GGC GGG GGG AGT GGC GGG AAT CTT
GTT CCT ATG GTT GCA ACA GTA GGA GGT TCC GGA GGG GGT GGC AGC GGA GGA
AAG CCA GTG TCC AAG ATG AGA ATG GCA ACC CCT TTG CTG ATG CAG GCC CTG
GGT GGC AGT CTG GGA GGT GGT GGC TCC GGC ATC GTA GGT ATA GTC GCC GGA
CTT GCA GTT TTG GCC GTG GTA GTG ATA GGC GCA GTT GTT GCC ACC GTT ATG
TGC CGA CGA AAG AGT TCA GGC GGC AAG GGT GGT TCT TAC TCC CAA GCT GCA
AGC TCC GAC TCC GCT CAG GGG AGT GAT GTT AGC TTG ACT GCA TGA

Supplemental Table 2. Nucleic acid sequence for assembled vaccine construct of Figure 1A.

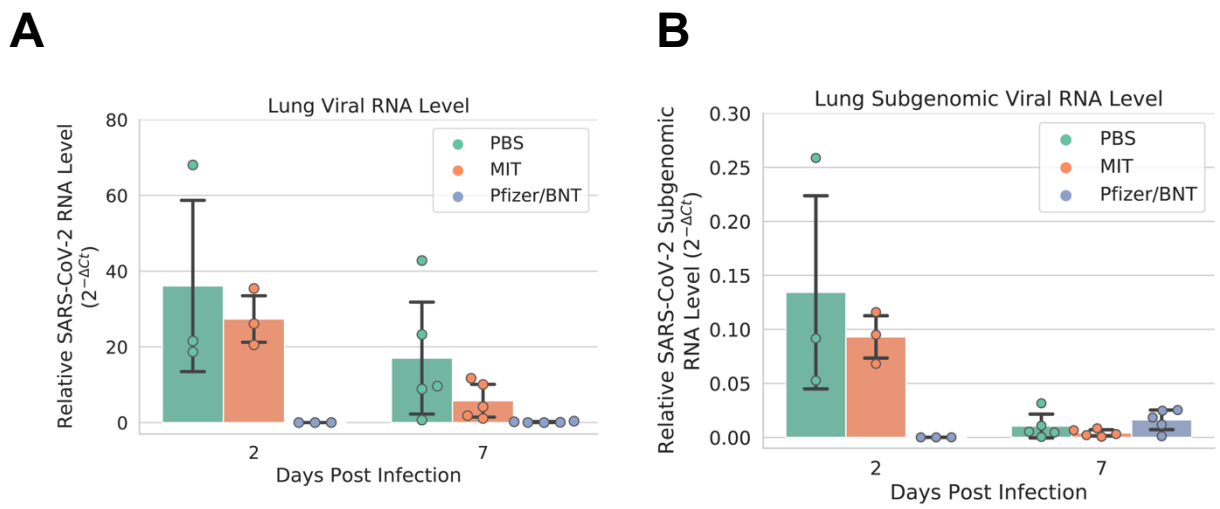

Supplemental Figure 1. (A) Lung viral RNA level, and (B) lung subgenomic viral RNA level. Error bars indicate the standard deviation around each mean.

2 DPI

7 DPI

a.
PBS

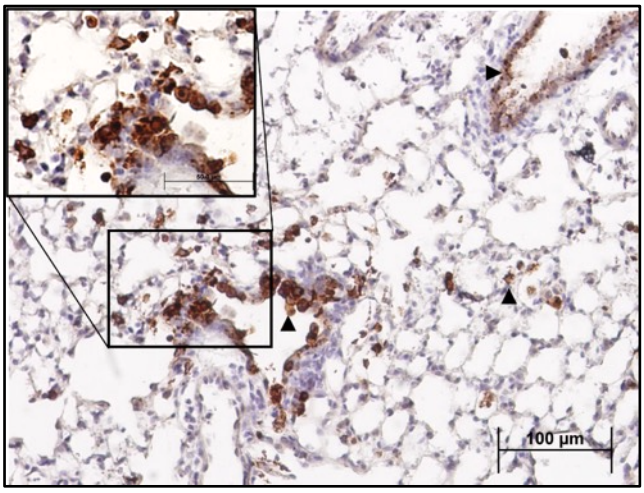

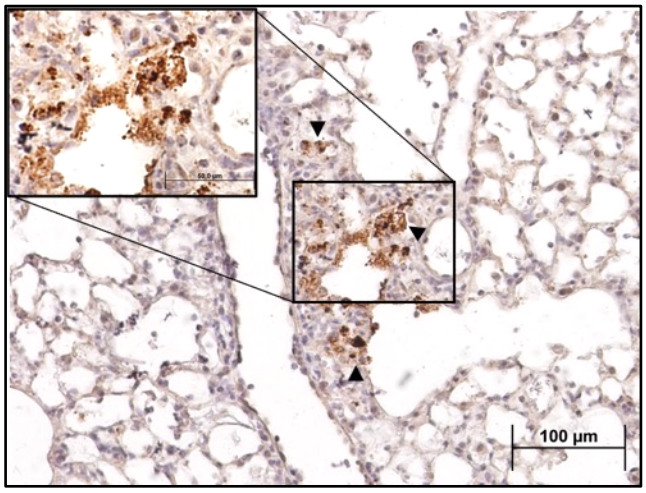

b.
MIT

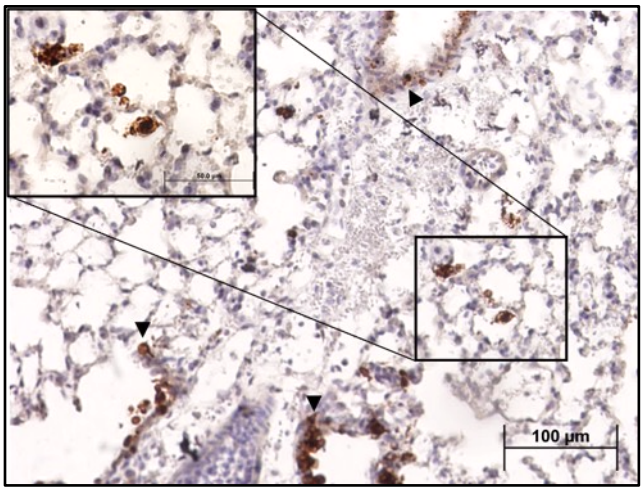

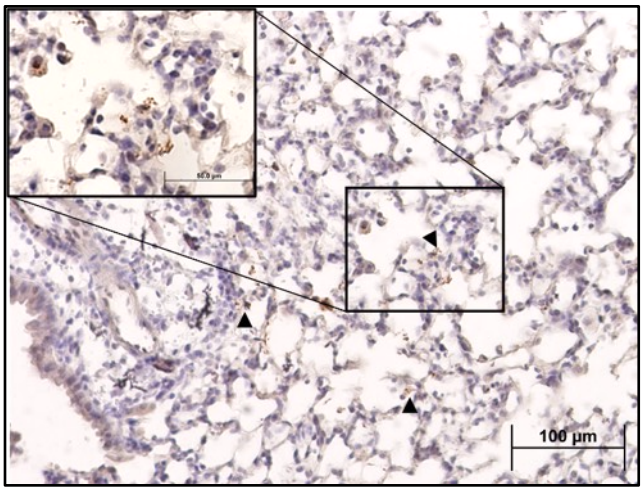

c.
Pfizer
BNT

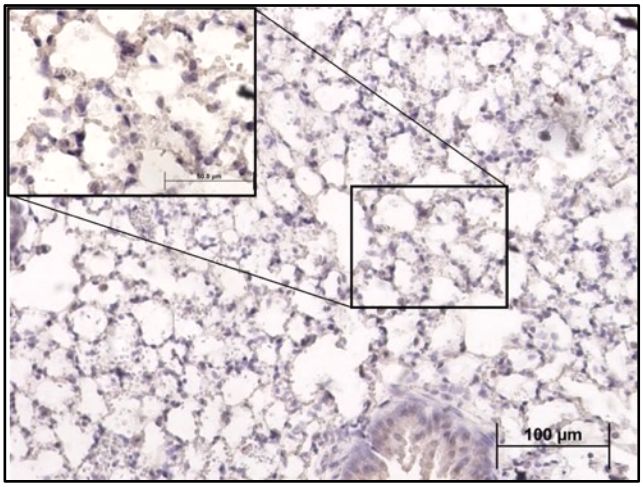

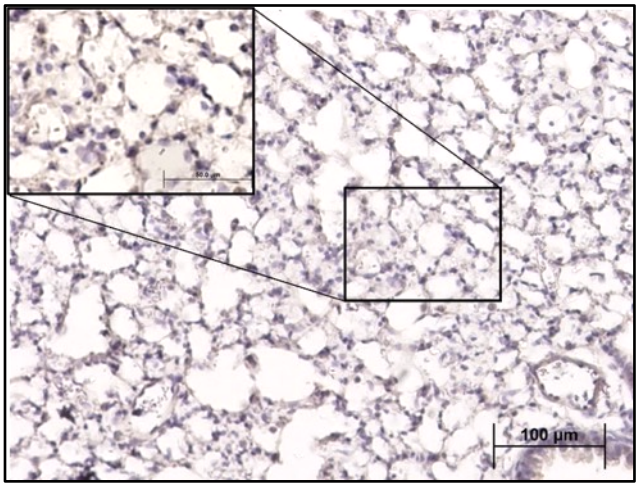

691 **Supplemental Figure 2.** All lung samples were subjected to IHC staining for SARS-CoV-2
692 spike protein (brown) with hematoxylin counterstain (blue), representative images of which are
693 shown here. Inset images taken at 40X magnification. Black arrowheads indicate selected areas
694 of viral infection. (a) Specimens vaccinated with PBS exhibited extensive staining indicative of
695 viral infection throughout the epithelium of both the bronchioles and the alveolar sacs, with the
696 viral infection appearing more intense at 2 days post-infection (dpi, left) than at 7 dpi (right).
697 Although viral infection is significantly reduced by 7 dpi, viral antigen was still readily detectable
698 throughout alveoli. (b) In comparison, specimens vaccinated with the MIT-T-COVID vaccine
699 exhibited similarly extensive viral infection at 2 dpi (left) throughout the bronchiolar and alveolar
700 epithelia, albeit somewhat reduced in intensity. However, by 7 dpi (right), viral infection was
701 significantly reduced in both extent and intensity, with brown puncta being detected only in a few
702 alveoli scattered throughout the tissue. (c) Contrasted with both PBS and MIT-T-COVID
703 vaccinated specimens, the Pfizer/BNT-vaccinated specimens exhibited significantly reduced
704 viral infections at both 2 (left) and 7 dpi (right). With the exception of a single area at 7 dpi (see
705 Supplemental Figure 3), viral antigen was undetected at both timepoints.

706

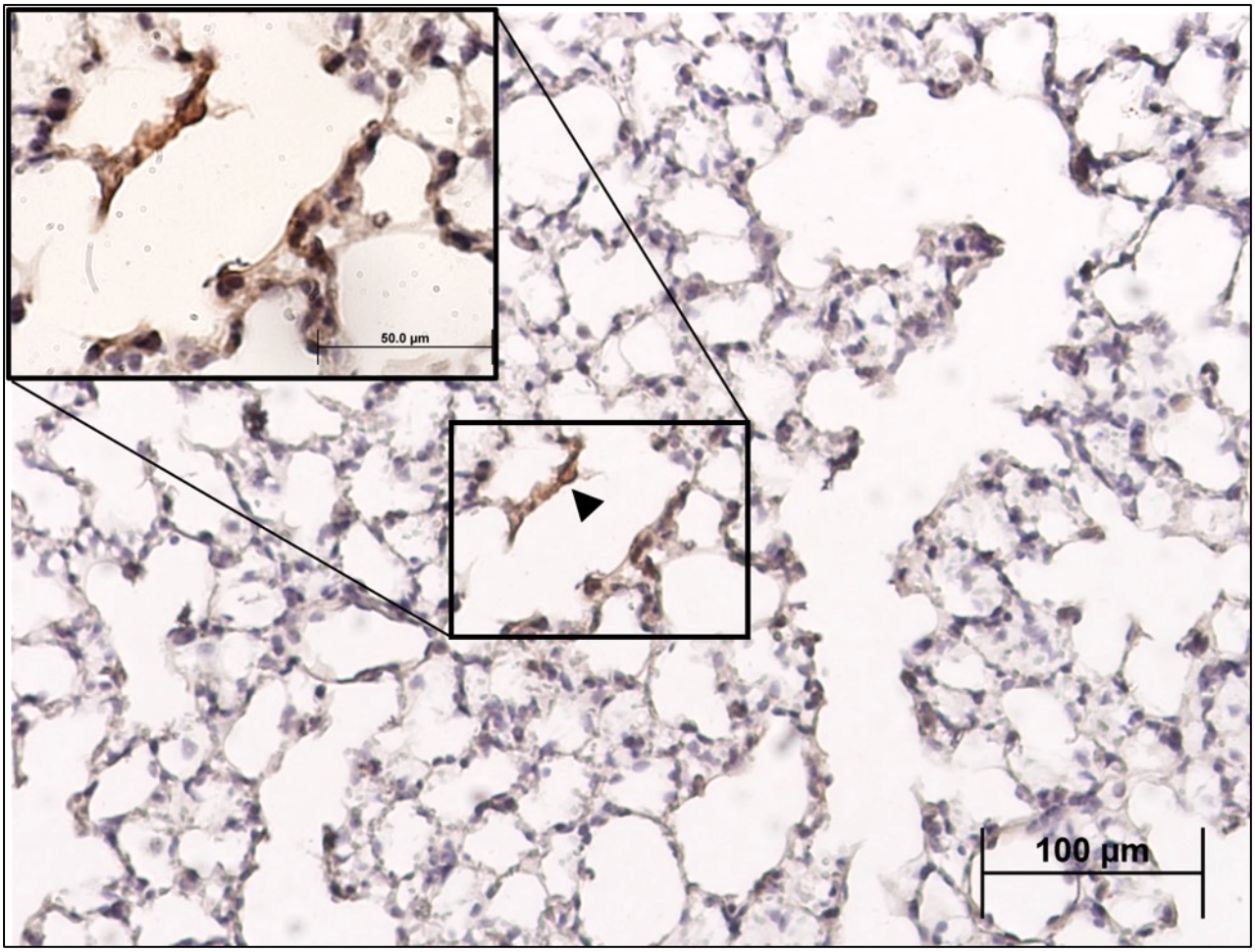

707

708

709 **Supplemental Figure 3.** Sole region of detectable SARS-CoV-2 spike antigen in alveoli of
710 Comirnaty® vaccinated lung specimens at 7 days post-infection. Black arrowhead indicates
711 infected cell.

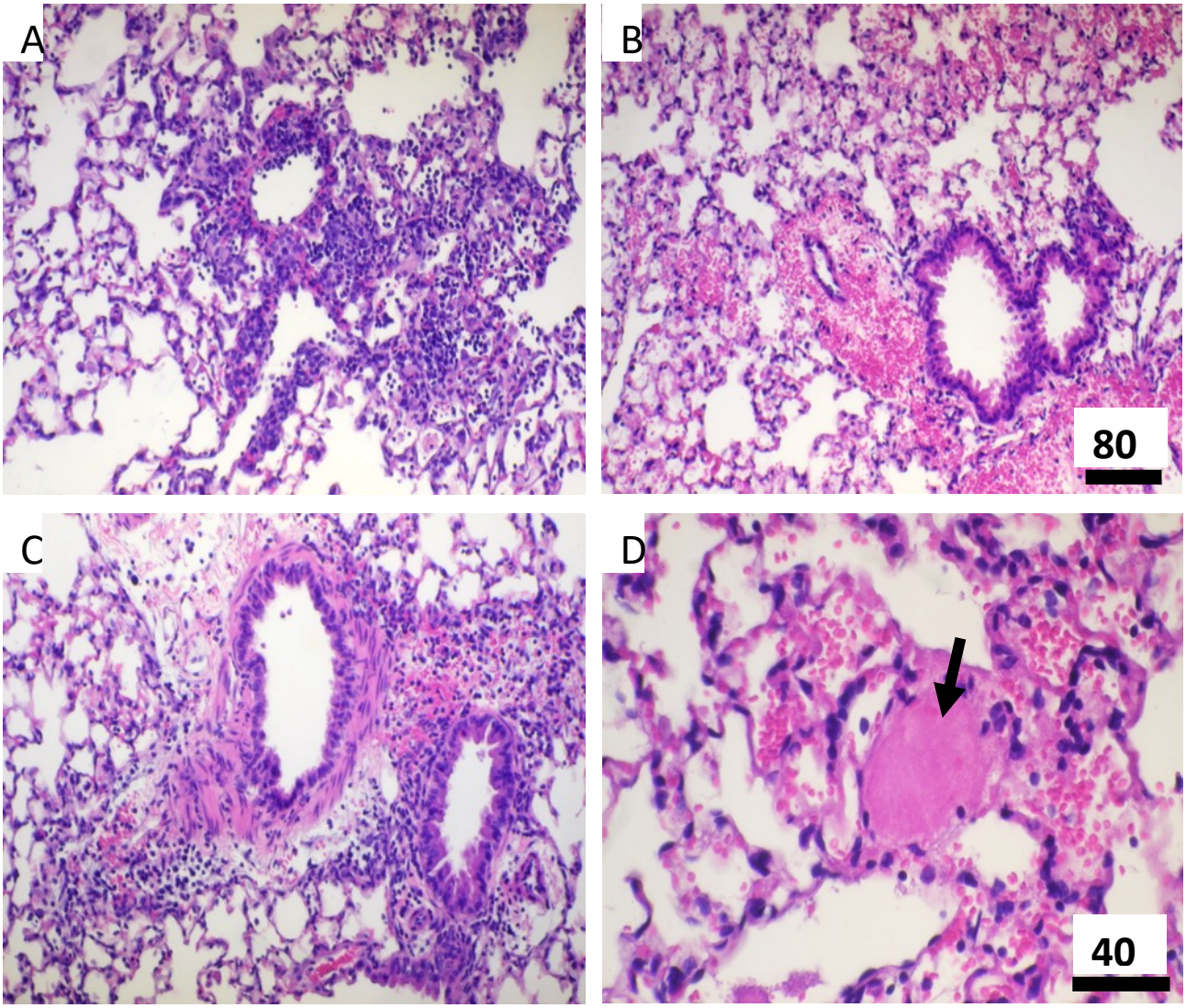

Supplemental Figure 4. Lung histopathology. Lungs of mice vaccinated with MIT-T-COVID (A) or Pfizer/BNT (B) are compared with those with PBS (C). At 7 dpi, the MIT-T-COVID vaccinated group showed extensive lymphocytic infiltrations in perivascular regions and spaces around bronchi, bronchioles, and alveoli. There are fewer infiltrations found in the Pfizer/BNT or PBS groups and they are only localized at perivascular regions around bronchi and large bronchioles. There is widespread congestion along with hemorrhage and few foci of thromboembolism (arrow in D) seen in the Pfizer/BNT group but not others. Bar = 80 μm in A, B and C; Bar = 40 μm in D.

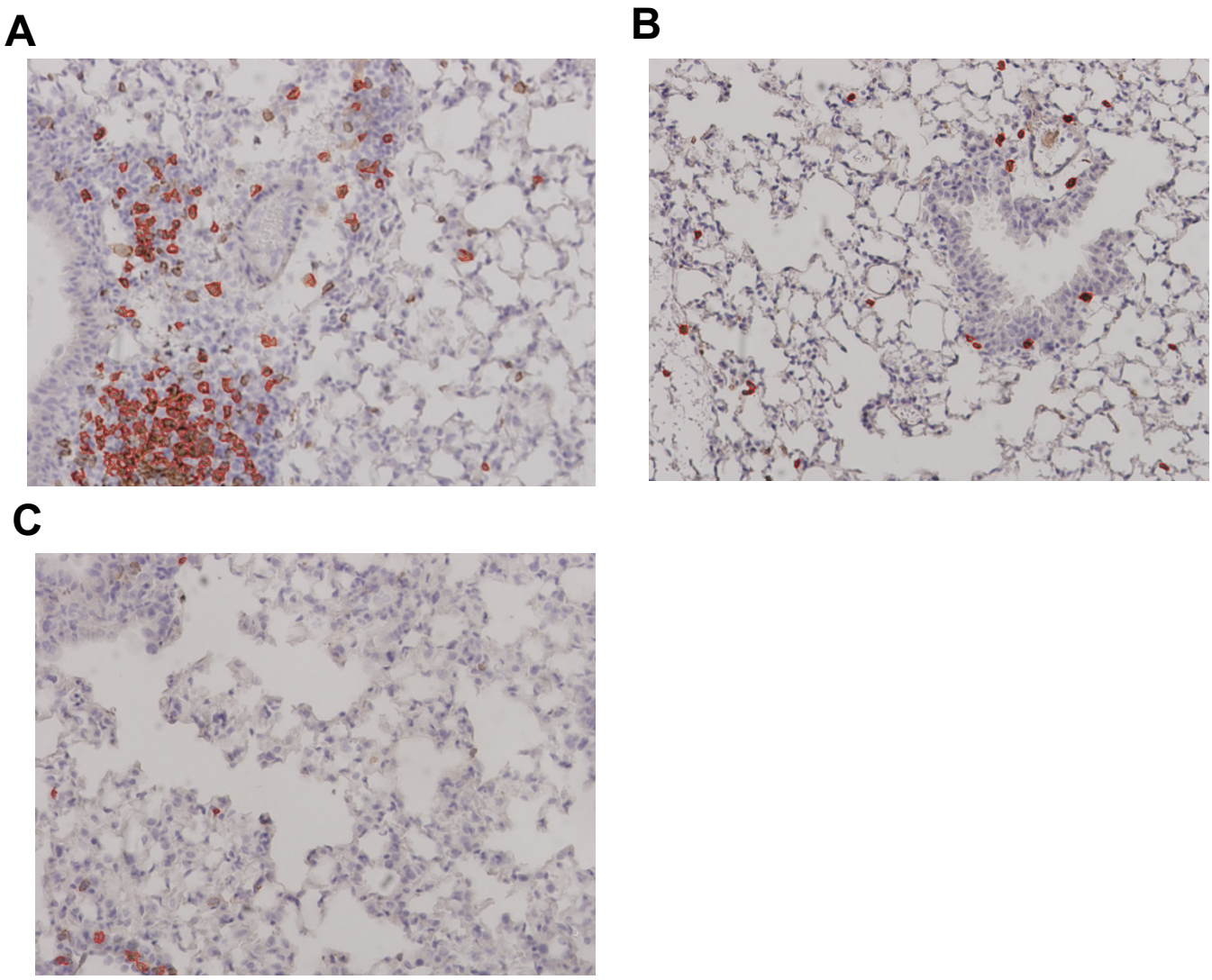

Supplemental Figure 5. Lung immunohistochemistry for $CD4^+$ cells at 7 dpi. Example $CD4^+$ stain images for (A) MIT-T-COVID, (B) Pfizer/BNT, and (C) PBS vaccinated animals. Lung samples were subjected to IHC staining for CD4 (brown) with hematoxylin counterstain (blue). Images were taken at 10X magnification. Red outlines indicate $CD4^+$ cells identified and counted by CellProfiler software (Methods). See also Figure 4 and Supplemental Figures 6-7.

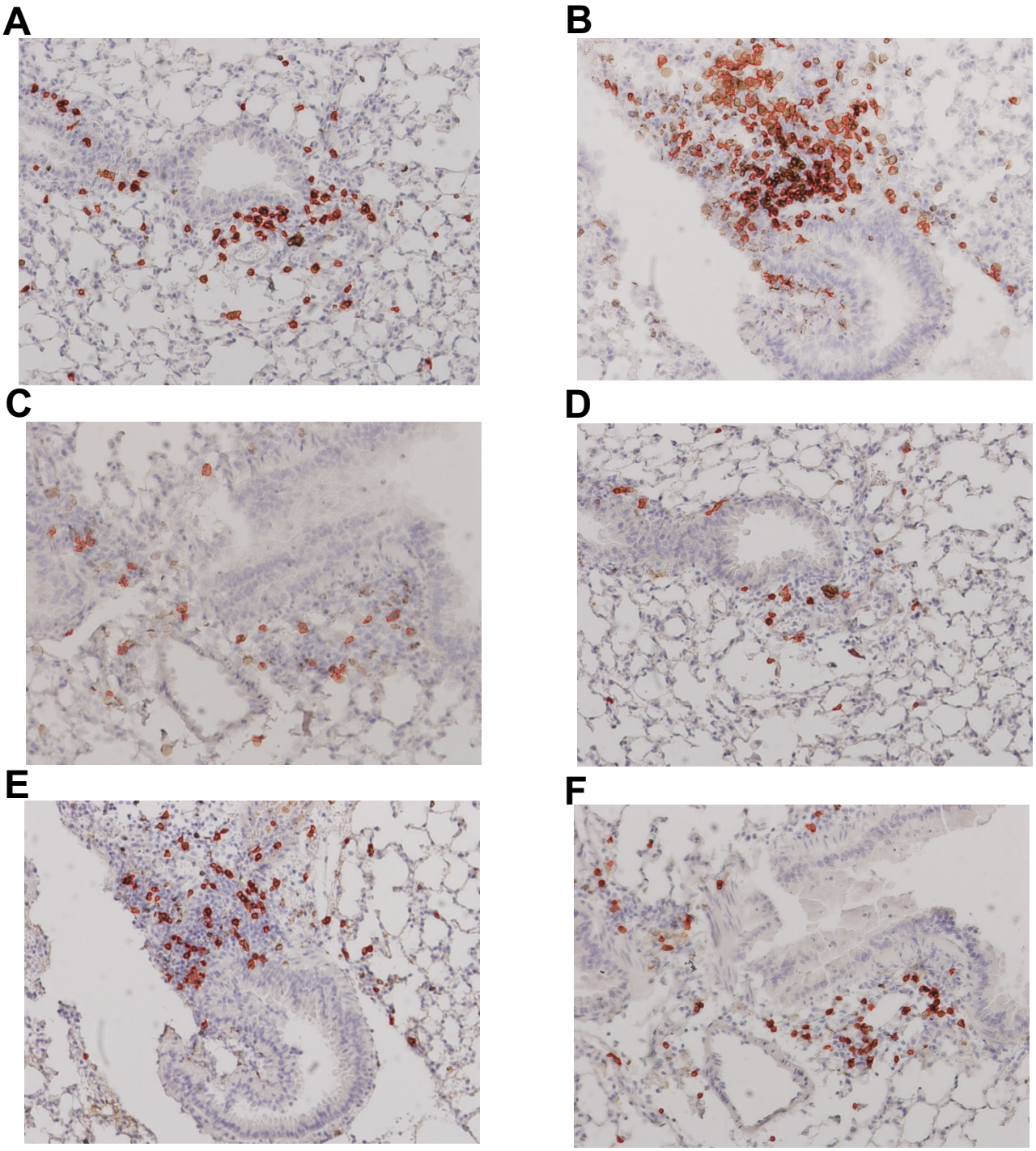

Supplemental Figure 6. Lung immunohistochemistry for $CD8^+$ and $CD4^+$ cells at 2 dpi. Example $CD8^+$ stain images for (A) MIT-T-COVID, (B) Pfizer/BNT, and (C) PBS vaccinated animals. Example $CD4^+$ stain images for (D) MIT-T-COVID, (E) Pfizer/BNT, and (F) PBS vaccinated animals. Lung samples were subjected to IHC staining for CD4 (brown) with hematoxylin counterstain (blue). Images were taken at 10X magnification. Red outlines indicate cells identified and counted by CellProfiler software (Methods). See also Figure 4, Supplemental Figure 5, and Supplemental Figure 7.

780 **Supplemental Figure 7.** Complete set of cell counts in lung immunohistochemistry images for
781 $CD8^+$ and $CD4^+$ cells at 2 and 7 dpi. Lung samples were subjected to IHC staining for CD4 or
782 CD8 (brown) with hematoxylin counterstain (blue). Images were taken at 10X magnification.
783 Red outlines indicate cells identified by CellProfiler software (Methods). See also Figure 4 and
784 Supplemental Figures 5-6.
785

References

1. Agrawal AS, Garron T, Tao X, Peng BH, Wakamiya M, Chan TS, Couch RB, Tseng CT. Generation of a transgenic mouse model of Middle East respiratory syndrome coronavirus infection and disease. J Virol. 2015 Apr;89(7):3659-70. doi: 10.1128/JVI.03427-14. Epub 2015 Jan 14. PMID: 25589660; PMCID: PMC4403411.

2. Baden LR, El Sahly HM, Essink B, Kotloff K, Frey S, Novak R, Diemert D, Spector SA, Rouphael N, Creech CB, McGettigan J, Khetan S, Segall N, Solis J, Brosz A, Fierro C, Schwartz H, Neuzil K, Corey L, Gilbert P, Janes H, Follmann D, Marovich M, Mascola J, Polakowski L, Ledgerwood J, Graham BS, Bennett H, Pajon R, Knightly C, Leav B, Deng W, Zhou H, Han S, Ivarsson M, Miller J, Zaks T; COVE Study Group. Efficacy and Safety of the mRNA-1273 SARS-CoV-2 Vaccine. N Engl J Med. 2021 Feb 4;384(5):403-416. doi: 10.1056/NEJMoa2035389. Epub 2020 Dec 30. PMID: 33378609; PMCID: PMC7787219.

3. Benjamini O, Rokach L, Itchaki G, Braester A, Shvidel L, Goldschmidt N, Shapira S, Dally N, Avigdor A, Rahav G, Lustig Y, Ben David SS, Fineman R, Paz A, Bairey O, Polliack A, Levy I, Tadmor T. Safety and efficacy of the BNT162b mRNA COVID-19 vaccine in patients with chronic lymphocytic leukemia. Haematologica. 2022 Mar 1;107(3):625-634. doi: 10.3324/haematol.2021.279196. PMID: 34320789; PMCID: PMC8883569.

4. Cohen AA, van Doremalen N, Greaney AJ, Andersen H, Sharma A, Starr TN, Keeffe JR, Fan C, Schulz JE, Gnanapragasam PNP, Kakutani LM, West AP Jr, Saturday G, Lee YE, Gao H, Jette CA, Lewis MG, Tan TK, Townsend AR, Bloom JD, Munster VJ, Bjorkman PJ. Mosaic RBD nanoparticles protect against challenge by diverse sarbecoviruses in animal models. Science. 2022 Aug 5;377(6606):eabq0839. doi: 10.1126/science.abq0839. Epub 2022 Aug 5. PMID: 35857620; PMCID: PMC9273039.

5. Croft NP, Smith SA, Pickering J, Sidney J, Peters B, Faridi P, Witney MJ, Sebastian P, Flesch IEA, Heading SL, Sette A, La Gruta NL, Purcell AW, Tscharke DC. Most viral peptides displayed by class I MHC on infected cells are immunogenic. Proc Natl Acad

Sci U S A. 2019 Feb 19;116(8):3112-3117. doi: 10.1073/pnas.1815239116. Epub 2019 Feb 4. PMID: 30718433; PMCID: PMC6386720.

6. de Silva TI, Liu G, Lindsey BB, Dong D, Moore SC, Hsu NS, Shah D, Wellington D, Mentzer AJ, Angyal A, Brown R, Parker MD, Ying Z, Yao X, Turtle L, Dunachie S; COVID-19 Genomics UK (COG-UK) Consortium, Maini MK, Ogg G, Knight JC; ISARIC4C Investigators, Peng Y, Rowland-Jones SL, Dong T. The impact of viral mutations on recognition by SARS-CoV-2 specific T cells. iScience. 2021 Nov 19;24(11):103353. doi: 10.1016/j.isci.2021.103353. Epub 2021 Oct 28. PMID: 34729465; PMCID: PMC8552693.

7. Ellis JM, Henson V, Slack R, Ng J, Hartzman RJ, Katovich Hurley C. Frequencies of HLA-A2 alleles in five U.S. population groups. Predominance Of A*02011 and identification of HLA-A*0231. Hum Immunol. 2000 Mar;61(3):334-40. doi: 10.1016/s0198-8859(99)00155-x. PMID: 10689125.

8. Geers D, Shamier MC, Bogers S, den Hartog G, Gommers L, Nieuwkoop NN, Schmitz KS, Rijsbergen LC, van Osch JAT, Dijkhuizen E, Smits G, Comvalius A, van Mourik D, Caniels TG, van Gils MJ, Sanders RW, Oude Munnink BB, Molenkamp R, de Jager HJ, Haagmans BL, de Swart RL, Koopmans MPG, van Binnendijk RS, de Vries RD, GeurtsvanKessel CH. SARS-CoV-2 variants of concern partially escape humoral but not T-cell responses in COVID-19 convalescent donors and vaccinees. Sci Immunol. 2021 May 25;6(59):eabj1750. doi: 10.1126/sciimmunol.abj1750. PMID: 34035118; PMCID: PMC9268159.

9. Hajnik RL, Plante JA, Liang Y, Alameh MG, Tang J, Bonam SR, Zhong C, Adam A, Scharton D, Rafael GH, Liu Y, Hazell NC, Sun J, Soong L, Shi PY, Wang T, Walker DH, Sun J, Weissman D, Weaver SC, Plante KS, Hu H. Dual spike and nucleocapsid mRNA vaccination confer protection against SARS-CoV-2 Omicron and Delta variants in preclinical models. Sci Transl Med. 2022 Sep 14;14(662):eabq1945. doi: 10.1126/scitranslmed.abq1945. Epub 2022 Sep 14. PMID: 36103514.

10. Heitmann JS, Bilich T, Tandler C, Nelde A, Maringer Y, Marconato M, Reusch J, Jäger S, Denk M, Richter M, Anton L, Weber LM, Roerden M, Bauer J, Rieth J, Wacker M, Hörber S, Peter A, Meisner C, Fischer I, Löffler MW, Karbach J, Jäger E, Klein R,

854 Rammensee HG, Salih HR, Walz JS. A COVID-19 peptide vaccine for the induction of
855 SARS-CoV-2 T cell immunity. Nature. 2022 Jan;601(7894):617-622. doi:
856 10.1038/s41586-021-04232-5. Epub 2021 Nov 23. PMID: 34814158; PMCID:
857 PMC8791831.
858
859 11. Israelow B, Mao T, Klein J, Song E, Menasche B, Omer SB, Iwasaki A. Adaptive
860 immune determinants of viral clearance and protection in mouse models of SARS-CoV-
861 2. Sci Immunol. 2021 Oct 15;6(64):eabl4509. doi: 10.1126/sciimmunol.abl4509. Epub
862 2021 Sep 2. PMID: 34623900; PMCID: PMC9047536.
863
864 12. Kared H, Redd AD, Bloch EM, Bonny TS, Sumatoh H, Kairi F, Carbajo D, Abel B, Newell
865 EW, Bettinotti MP, Benner SE, Patel EU, Littlefield K, Laeyendecker O, Shoham S,
866 Sullivan D, Casadevall A, Pekosz A, Nardin A, Fehlings M, Tobian AA, Quinn TC.
867 SARS-CoV-2-specific CD8+ T cell responses in convalescent COVID-19 individuals. J
868 Clin Invest. 2021 Mar 1;131(5):e145476. doi: 10.1172/JCI145476. PMID: 33427749;
869 PMCID: PMC7919723.
870
871 13. Kingstad-Bakke B, Lee W, Chandrasekar SS, Gasper DJ, Salas-Quinchucua C, Cleven
872 T, Sullivan JA, Talaat A, Osorio JE, Suresh M. Vaccine-induced systemic and mucosal T
873 cell immunity to SARS-CoV-2 viral variants. Proc Natl Acad Sci U S A. 2022 May
874 17;119(20):e2118312119. doi: 10.1073/pnas.2118312119. Epub 2022 May 13. PMID:
875 35561224; PMCID: PMC9171754.
876
877 14. Kotturi MF, Assarsson E, Peters B, Grey H, Oseroff C, Pasquetto V, Sette A. Of mice
878 and humans: how good are HLA transgenic mice as a model of human immune
879 responses? Immunome Res. 2009 Jun 17;5:3. doi: 10.1186/1745-7580-5-3. PMID:
880 19534819; PMCID: PMC2702351.
881
882 15. Kreiter S, Selmi A, Diken M, Sebastian M, Osterloh P, Schild H, Huber C, Türeci O,
883 Sahin U. Increased antigen presentation efficiency by coupling antigens to MHC class I
884 trafficking signals. J Immunol. 2008 Jan 1;180(1):309-18. doi:
885 10.4049/jimmunol.180.1.309. Erratum in: J Immunol. 2012 Sep 1;189(5):2682. PMID:
886 18097032.
887

16. Kumari P, Rothan HA, Natekar JP, Stone S, Pathak H, Strate PG, Arora K, Brinton MA, Kumar M. Neuroinvasion and Encephalitis Following Intranasal Inoculation of SARS-CoV-2 in K18-hACE2 Mice. Viruses. 2021 Jan 19;13(1):132. doi: 10.3390/v13010132. PMID: 33477869; PMCID: PMC7832889.

17. Liu G, Carter B, Bricken T, Jain S, Viard M, Carrington M, Gifford DK. Computationally Optimized SARS-CoV-2 MHC Class I and II Vaccine Formulations Predicted to Target Human Haplotype Distributions. Cell Syst. 2020 Aug 26;11(2):131-144.e6. doi: 10.1016/j.cels.2020.06.009. Epub 2020 Jul 27. PMID: 32721383; PMCID: PMC7384425.

18. Liu G, Carter B, Gifford DK. Predicted Cellular Immunity Population Coverage Gaps for SARS-CoV-2 Subunit Vaccines and Their Augmentation by Compact Peptide Sets. Cell Syst. 2021 Jan 20;12(1):102-107.e4. doi: 10.1016/j.cels.2020.11.010. Epub 2020 Nov 27. PMID: 33321075; PMCID: PMC7691134.

19. Liu, G., Carter B., Dimitrakakis A., Gifford D. K. Maximum n-times Coverage for Vaccine Design, International Conference on Learning Representations, ICLR (2022), https://arxiv.org/abs/2101.10902

20. Martinez DR, Schäfer A, Leist SR, De la Cruz G, West A, Atochina-Vasserman EN, Lindesmith LC, Pardi N, Parks R, Barr M, Li D, Yount B, Saunders KO, Weissman D, Haynes BF, Montgomery SA, Baric RS. Chimeric spike mRNA vaccines protect against Sarbecovirus challenge in mice. Science. 2021 Aug 27;373(6558):991-998. doi: 10.1126/science.abi4506. Epub 2021 Jun 22. PMID: 34214046; PMCID: PMC8899822.

21. Matchett WE, Joag V, Stolley JM, Shepherd FK, Quarnstrom CF, Mickelson CK, Wijeyesinghe S, Soerens AG, Becker S, Thiede JM, Weyu E, O'Flanagan S, Walter JA, Vu MN, Menachery VD, Bold TD, Vezys V, Jenkins MK, Langlois RA, Masopust D. Nucleocapsid vaccine elicits spike-independent SARS-CoV-2 protective immunity. J Immunol. 2021 Jun 30;: PMID: 33948591; PMCID: PMC8095198.

22. Moss P. The T cell immune response against SARS-CoV-2. Nat Immunol. 2022 Feb;23(2):186-193. doi: 10.1038/s41590-021-01122-w. Epub 2022 Feb 1. PMID: 35105982.

23. Nakiboneka R, Mugaba S, Auma BO, Kintu C, Lindan C, Nanteza MB, Kaleebu P, Serwanga J. Interferon gamma (IFN-γ) negative CD4+ and CD8+ T-cells can produce immune mediators in response to viral antigens. Vaccine. 2019 Jan 3;37(1):113-122. doi: 10.1016/j.vaccine.2018.11.024. Epub 2018 Nov 17. PMID: 30459072; PMCID: PMC6290111.

24. Nathan A, Rossin EJ, Kaseke C, Park RJ, Khatri A, Koundakjian D, Urbach JM, Singh NK, Bashirova A, Tano-Menka R, Senjobe F, Waring MT, Piechocka-Trocha A, Garcia-Beltran WF, Iafrate AJ, Naranbhai V, Carrington M, Walker BD, Gaiha GD. Structure-guided T cell vaccine design for SARS-CoV-2 variants and sarbecoviruses. Cell. 2021 Aug 19;184(17):4401-4413.e10. doi: 10.1016/j.cell.2021.06.029. Epub 2021 Jun 30. PMID: 34265281; PMCID: PMC8241654.

25. O'Donnell TJ, Rubinsteyn A, Laserson U. MHCflurry 2.0: Improved Pan-Allele Prediction of MHC Class I-Presented Peptides by Incorporating Antigen Processing. Cell Syst. 2020 Jul 22;11(1):42-48.e7. doi: 10.1016/j.cels.2020.06.010. Epub 2020 Jul 14. Erratum in: Cell Syst. 2020 Oct 21;11(4):418-419. PMID: 32711842.

26. Pardi N, Hogan MJ, Pelc RS, Muramatsu H, Andersen H, DeMaso CR, Dowd KA, Sutherland LL, Scearce RM, Parks R, Wagner W, Granados A, Greenhouse J, Walker M, Willis E, Yu JS, McGee CE, Sempowski GD, Mui BL, Tam YK, Huang YJ, Vanlandingham D, Holmes VM, Balachandran H, Sahu S, Lifton M, Higgs S, Hensley SE, Madden TD, Hope MJ, Karikó K, Santra S, Graham BS, Lewis MG, Pierson TC, Haynes BF, Weissman D. Zika virus protection by a single low-dose nucleoside-modified mRNA vaccination. Nature. 2017 Mar 9;543(7644):248-251. doi: 10.1038/nature21428. Epub 2017 Feb 2. PMID: 28151488; PMCID: PMC5344708.

27. Pardieck IN, van der Sluis TC, van der Gracht ETI, Veerkamp DMB, Behr FM, van Duikeren S, Beyrend G, Rip J, Nadafi R, Beyranvand Nejad E, Mülling N, Brasem DJ, Camps MGM, Myeni SK, Bredenbeek PJ, Kikkert M, Kim Y, Cicin-Sain L, Abdelaal T, van Gisbergen KPJM, Franken KLMC, Drijfhout JW, Melief CJM, Zondag GCM, Ossendorp F, Arens R. A third vaccination with a single T cell epitope confers protection

955 in a murine model of SARS-CoV-2 infection. Nat Commun. 2022 Jul 8;13(1):3966. doi:
956 10.1038/s41467-022-31721-6. PMID: 35803932; PMCID: PMC9267705.
957
958 28. Redd AD, Nardin A, Kared H, Bloch EM, Pekosz A, Laeyendecker O, Abel B, Fehlings
959 M, Quinn TC, Tobian AA. CD8+ T cell responses in COVID-19 convalescent individuals
960 target conserved epitopes from multiple prominent SARS-CoV-2 circulating variants.
961 medRxiv [Preprint]. 2021 Feb 12:2021.02.11.21251585. doi:
962 10.1101/2021.02.11.21251585. Update in: Open Forum Infect Dis. 2021 Mar
963 30;8(7):ofab143. PMID: 33594378; PMCID: PMC7885937.
964
965 29. Reynisson B, Alvarez B, Paul S, Peters B, Nielsen M. NetMHCpan-4.1 and
966 NetMHCIIpan-4.0: improved predictions of MHC antigen presentation by concurrent
967 motif deconvolution and integration of MS MHC eluted ligand data. Nucleic Acids Res.
968 2020 Jul 2;48(W1):W449-W454. doi: 10.1093/nar/gkaa379. PMID: 32406916; PMCID:
969 PMC7319546.
970
971 30. Sahin U, Derhovanessian E, Miller M, Kloke BP, Simon P, Löwer M, Bukur V, Tadmor
972 AD, Luxemburger U, Schrörs B, Omokoko T, Vormehr M, Albrecht C, Paruzynski A,
973 Kuhn AN, Buck J, Heesch S, Schreeb KH, Müller F, Ortseifer I, Vogler I, Godehardt E,
974 Attig S, Rae R, Breitkreuz A, Tolliver C, Suchan M, Martic G, Hohberger A, Sorn P,
975 Diekmann J, Ciesla J, Waksmann O, Brück AK, Witt M, Zillgen M, Rothermel A,
976 Kasemann B, Langer D, Bolte S, Diken M, Kreiter S, Nemecek R, Gebhardt C, Grabbe
977 S, Höller C, Utikal J, Huber C, Loquai C, Türeci Ö. Personalized RNA mutanome
978 vaccines mobilize poly-specific therapeutic immunity against cancer. Nature. 2017 Jul
979 13;547(7662):222-226. doi: 10.1038/nature23003. Epub 2017 Jul 5. PMID: 28678784.
980
981 31. Seabold, S., Perktold, J. Statsmodels: Econometric and statistical modeling with python.
982 Proceedings of the 9th Python in Science Conference. 2010; 57(61).
983
984 32. Sekine T, Perez-Potti A, Rivera-Ballesteros O, Strålin K, Gorin JB, Olsson A, Llewellyn-
985 Lacey S, Kamal H, Bogdanovic G, Muschiol S, Wullimann DJ, Kammann T, Emgård J,
986 Parrot T, Folkesson E; Karolinska COVID-19 Study Group, Rooyackers O, Eriksson LI,
987 Henter JI, Sönnerborg A, Allander T, Albert J, Nielsen M, Klingström J, Gredmark-Russ
988 S, Björkström NK, Sandberg JK, Price DA, Ljunggren HG, Aleman S, Buggert M. Robust

T Cell Immunity in Convalescent Individuals with Asymptomatic or Mild COVID-19. Cell. 2020 Oct 1;183(1):158-168.e14. doi: 10.1016/j.cell.2020.08.017. Epub 2020 Aug 14. PMID: 32979941; PMCID: PMC7427556.

33. Shuai H, Chan JF, Yuen TT, Yoon C, Hu JC, Wen L, Hu B, Yang D, Wang Y, Hou Y, Huang X, Chai Y, Chan CC, Poon VK, Lu L, Zhang RQ, Chan WM, Ip JD, Chu AW, Hu YF, Cai JP, Chan KH, Zhou J, Sridhar S, Zhang BZ, Yuan S, Zhang AJ, Huang JD, To KK, Yuen KY, Chu H. Emerging SARS-CoV-2 variants expand species tropism to murines. EBioMedicine. 2021 Nov;73:103643. doi: 10.1016/j.ebiom.2021.103643. Epub 2021 Oct 21. PMID: 34689086; PMCID: PMC8530107.

34. Snyder TM, Gittelman RM, Klinger M, May DH, Osborne EJ, Taniguchi R, Zahid HJ, Kaplan IM, Dines JN, Noakes MT, Pandya R, Chen X, Elasady S, Svejnoha E, Ebert P, Pesesky MW, De Almeida P, O'Donnell H, DeGottardi Q, Keitany G, Lu J, Vong A, Elyanow R, Fields P, Greissl J, Baldo L, Semprini S, Cerchione C, Nicolini F, Mazza M, Delmonte OM, Dobbs K, Laguna-Goya R, Carreño-Tarragona G, Barrio S, Imberti L, Sottini A, Quiros-Roldan E, Rossi C, Biondi A, Bettini LR, D'Angio M, Bonfanti P, Tompkins MF, Alba C, Dalgard C, Sambri V, Martinelli G, Goldman JD, Heath JR, Su HC, Notarangelo LD, Paz-Artal E, Martinez-Lopez J, Carlson JM, Robins HS. Magnitude and Dynamics of the T-Cell Response to SARS-CoV-2 Infection at Both Individual and Population Levels. medRxiv [Preprint]. 2020 Sep 17:2020.07.31.20165647. doi: 10.1101/2020.07.31.20165647. PMID: 32793919; PMCID: PMC7418734.

35. Stirling DR, Swain-Bowden MJ, Lucas AM, Carpenter AE, Cimini BA, Goodman A. CellProfiler 4: improvements in speed, utility and usability. BMC Bioinformatics. 2021 Sep 10;22(1):433. doi: 10.1186/s12859-021-04344-9. PMID: 34507520; PMCID: PMC8431850.

36. Swank Z, Senussi Y, Manickas-Hill Z, Yu XG, Li JZ, Alter G, Walt DR. Persistent circulating SARS-CoV-2 spike is associated with post-acute COVID-19 sequelae. Clin Infect Dis. 2022 Sep 2:ciac722. doi: 10.1093/cid/ciac722. Epub ahead of print. PMID: 36052466.

37. Tregoning JS, Flight KE, Higham SL, Wang Z, Pierce BF. Progress of the COVID-19 vaccine effort: viruses, vaccines and variants versus efficacy, effectiveness and escape. Nat Rev Immunol. 2021 Oct;21(10):626-636. doi: 10.1038/s41577-021-00592-1. Epub 2021 Aug 9. PMID: 34373623; PMCID: PMC8351583.

38. Tseng CTK, Huang C, Newman P, Wang N, Narayanan K, Watts DM, Makino S, Packard M, Zaki SR, Chan TS, and Peters CJ. 2007. SARS Coronavirus Infection of Transgenic Mice bearing the Human Angiotensin Converting Enzyme 2 (hACE2) Virus Receptor. *JVI* 81: 1162-1173.

39. Tseng CT, Sbrana E, Iwata-Yoshikawa N, Newman PC, Garron T, Atmar RL, Peters CJ, Couch RB. Immunization with SARS coronavirus vaccines leads to pulmonary immunopathology on challenge with the SARS virus. PLoS One. 2012;7(4):e35421. doi: 10.1371/journal.pone.0035421. Epub 2012 Apr 20. Erratum in: PLoS One. 2012;7(8). doi:10.1371/annotation/2965cfae-b77d-4014-8b7b-236e01a35492. PMID: 22536382; PMCID: PMC3335060.

40. UniProt Consortium. UniProt: a worldwide hub of protein knowledge. Nucleic Acids Res. 2019 Jan 8;47(D1):D506-D515. doi: 10.1093/nar/gky1049. PMID: 30395287; PMCID: PMC6323992.

41. Virtanen P, Gommers R, Oliphant TE, Haberland M, Reddy T, Cournapeau D, Burovski E, Peterson P, Weckesser W, Bright J, van der Walt SJ, Brett M, Wilson J, Millman KJ, Mayorov N, Nelson ARJ, Jones E, Kern R, Larson E, Carey CJ, Polat İ, Feng Y, Moore EW, VanderPlas J, Laxalde D, Perktold J, Cimrman R, Henriksen I, Quintero EA, Harris CR, Archibald AM, Ribeiro AH, Pedregosa F, van Mulbregt P; SciPy 1.0 Contributors. SciPy 1.0: fundamental algorithms for scientific computing in Python. Nat Methods. 2020 Mar;17(3):261-272. doi: 10.1038/s41592-019-0686-2. Epub 2020 Feb 3. Erratum in: Nat Methods. 2020 Feb 24;: PMID: 32015543; PMCID: PMC7056644.

42. Vita R, Mahajan S, Overton JA, Dhanda SK, Martini S, Cantrell JR, Wheeler DK, Sette A, Peters B. The Immune Epitope Database (IEDB): 2018 update. Nucleic Acids Res. 2018 Oct 24. doi: 10.1093/nar/gky1006. [Epub ahead of print] PubMed PMID: 30357391.

1056 43. Walsh EE, Frenck RW Jr, Falsey AR, Kitchin N, Absalon J, Gurtman A, Lockhart S,
1057 Neuzil K, Mulligan MJ, Bailey R, Swanson KA, Li P, Koury K, Kalina W, Cooper D,
1058 Fontes-Garfias C, Shi PY, Türeci Ö, Tompkins KR, Lyke KE, Raabe V, Dormitzer PR,
1059 Jansen KU, Şahin U, Gruber WC. Safety and Immunogenicity of Two RNA-Based Covid-
1060 19 Vaccine Candidates. N Engl J Med. 2020 Dec 17;383(25):2439-2450. doi:
1061 10.1056/NEJMoa2027906. Epub 2020 Oct 14. PMID: 33053279; PMCID: PMC7583697.
1062
1063 44. Willett BJ, Grove J, MacLean OA, Wilkie C, De Lorenzo G, Furnon W, Cantoni D, Scott
1064 S, Logan N, Ashraf S, Manali M, Szemiel A, Cowton V, Vink E, Harvey WT, Davis C,
1065 Asamaphan P, Smollett K, Tong L, Orton R, Hughes J, Holland P, Silva V, Pascall DJ,
1066 Puxty K, da Silva Filipe A, Yebra G, Shaaban S, Holden MTG, Pinto RM, Gunson R,
1067 Templeton K, Murcia PR, Patel AH, Klenerman P, Dunachie S; PITCH Consortium;
1068 COVID-19 Genomics UK (COG-UK) Consortium, Haughney J, Robertson DL, Palmarini
1069 M, Ray S, Thomson EC. SARS-CoV-2 Omicron is an immune escape variant with an
1070 altered cell entry pathway. Nat Microbiol. 2022 Aug;7(8):1161-1179. doi:
1071 10.1038/s41564-022-01143-7. Epub 2022 Jul 7. PMID: 35798890; PMCID:
1072 PMC9352574.
1073
1074 45. World Health Organization (WHO). In the wake of the pandemic: preparing for Long
1075 COVID (2021). Policy Brief 39. Accessed August 14, 2022.
1076 https://apps.who.int/iris/bitstream/handle/10665/339629/Policy-brief-39-1997-8073-
1077 eng.pdf
1078
1079 46. Zeng H, Gifford DK. Quantification of Uncertainty in Peptide-MHC Binding Prediction
1080 Improves High-Affinity Peptide Selection for Therapeutic Design. Cell Syst. 2019 Aug
1081 28;9(2):159-166.e3. doi: 10.1016/j.cels.2019.05.004. Epub 2019 Jun 5. PMID:
1082 31176619; PMCID: PMC6715517.
1083
1084 47. Zhang X, Wu S, Wu B, Yang Q, Chen A, Li Y, Zhang Y, Pan T, Zhang H, He X. SARS-
1085 CoV-2 Omicron strain exhibits potent capabilities for immune evasion and viral entrance.
1086 Signal Transduct Target Ther. 2021 Dec 17;6(1):430. doi: 10.1038/s41392-021-00852-5.
1087 PMID: 34921135; PMCID: PMC8678971.
1088

1089 48. Zhao J, Zhao J, Mangalam AK, Channappanavar R, Fett C, Meyerholz DK, Agnihothram
1090 S, Baric RS, David CS, Perlman S. Airway Memory CD4(+) T Cells Mediate Protective
1091 Immunity against Emerging Respiratory Coronaviruses. Immunity. 2016 Jun
1092 21;44(6):1379-91. doi: 10.1016/j.immuni.2016.05.006. Epub 2016 Jun 7. PMID:
1093 27287409; PMCID: PMC4917442.